Energy 55 (2013) 278–294

Contents lists available at SciVerse ScienceDirect

Energy

journal homepage: www.elsevier.com/locate/energy

A theoretical study on the use of microwaves in reducing energy consumption for an endothermic reaction: Role of metal coated bounding surface

Madhuchhanda Bhattacharya [a], Tanmay Basak [b,*]

[a] C2-5-4C, Delhi Avenue, Indian Institute of Technology Madras Campus, Chennai 600036, India
[b] Department of Chemical Engineering, Indian Institute of Technology Madras, Chennai 600036, India

ARTICLE INFO

Article history:
Received 4 September 2012
Received in revised form
27 February 2013
Accepted 3 March 2013
Available online 25 April 2013

Keywords:
Reaction
Microwave
Metallic support
Mathematical modeling
Energy savings

ABSTRACT

This work presents a theoretical analysis on savings of energy during an endothermic reaction under microwave heating compared to conventional heating and shows the use of metal coated bounding surface to enhance the energy savings in otherwise low saving zones. Main thrust of this work is the quantification of energy savings for various probable microwave heating scenarios that may arise either due to varying reactor dimension ($2L$) over *thin*, *intermediate* and *thick* regimes or due to varying dielectric properties of the reactor. The analysis considers detailed transport equations in conjunction with Helmholtz equation for microwave propagation within a semiinfinite batch reactor. Simulations show that use of microwave can significantly save energy (as high as 60%) depending on reactor configuration. Simulations also show efficient use of metal coated bounding surface to enhance energy savings for reactors with $2L/\lambda_{\text{eff}} = 0.5n - 0.25$, where $n = 1, 2, 3\ldots$ and λ_{eff} is wavelength of microwave within the reactor. The enhancement is found to be 2 and 1.5 times at $2L/\lambda_{\text{eff}} = 0.25$ and 0.75, respectively. Various regions of efficient use of metal coated bounding surface for different microwave heating scenarios have been identified in a series of master curves.

© 2013 Published by Elsevier Ltd.

1. Introduction

Energy consumption has been one of the important issues over past few decades triggering a series of research on finding faster and lower energy consuming technologies. Among several other possibilities like ultrasonic [1–16], electro-osmotic [17–20] and pulsed corona processing [21–26], microwave processing of materials came out as an alternate viable process due to its faster processing and quick start up capabilities. Microwaves within frequency range of 300 MHz to 300 GHz interact with dipoles and can transfer energy volumetrically at molecular level in dielectric materials. Volumetric supply of energy accelerates the progress of a process due to lower energy transfer time compared to cases where energy is supplied from surfaces. Over the years, potentials of microwave processing in terms of process intensification and lower energy consumption have been proven in many different fields [27–39] with a major potential in the field of material synthesis, where chemical reactions are reported to undergo dramatic acceleration under microwave radiations [40–60].

Since reaction rates are strong functions of local temperature, a detailed knowledge about temperature profile inside the reacting domain is necessary to ascertain and quantify enhancement of reaction under microwave radiation. The situation becomes more demanding for endothermic reaction, where occurrence of reaction depends on local availability of heat and hence on heating pattern. It may be noted that microwave induced heating pattern may be highly complex with multiple local hot-spots within the domain depending on dimension and dielectric properties of the medium [61–65]. However, due to the difficulties associated with detailed measurement of electric field within the domain, microwave induced heating pattern has often been approximated by ad hoc models in literature. Use of such ad hoc models may hide some of the physics underlying the observed enhancement leading to speculation about athermal effect of microwave radiation on chemical reaction [66,67]. Correspondingly, a few theoretical studies have been initiated to relate the enhanced reaction rate due to microwave heating effects [68–73]. But, none of the earlier researchers considered detailed description of microwave propagation via Helmholtz equation and thus could not quantify/analyze

---

* Corresponding author.
E-mail address: tanmay@iitm.ac.in (T. Basak).

0360-5442/$ – see front matter © 2013 Published by Elsevier Ltd.
http://dx.doi.org/10.1016/j.energy.2013.03.016

Nomenclature

C_A and c_A	dimensional (mol/m^3) and dimensionless reactant concentration
C_{A0}	initial reactant concentration (mol/m^3)
$\bar{c}_A$	dimensionless average reactant concentration
$(\rho C_p)_{\text{eff}}$	effective heat capacity (J/m^{3}K)
D_{eff}	effective reactant diffusivity within packed bed (m^2/s)
$D_{p_{\text{eff}}}$	effective penetration depth (m)
E	activation energy (kJ/kmol)
E_m	electric field (V/m)
f	frequency (Hz)
f_p	$\lambda_{\text{eff}}/2\pi D_{p_{\text{eff}}}$
f_w	$\lambda_{\text{eff}}/\lambda_0$
I_0	intensity of incident radiation (W/m^2)
k_{eff}	effective thermal conductivity of packed bed (W/m K)
L	half-width of packed column, m
N_p	penetration number ($2L/D_{p_{\text{eff}}}$)
N_R	heat-reaction number ($2L\Delta H_R \phi R(C_{A0}, T_0)/I_0$)
N_w	wave number ($2L/\lambda_{\text{eff}}$)
Q_{MW} and q_{MW}	dimensional (W/m^3) and dimensionless absorbed power distribution
$\bar{q}_{\text{MW}}$	dimensionless average absorbed power
t	time, s
T	temperature, K
T_0	initial temperature, K
Z and z	dimensional (m) and dimensionless spatial coordinate

Greek symbols

α_{eff}	effective thermal conductivity ($k_{\text{eff}}/(\rho C_p)_{\text{eff}}$)
β	conduction number ($k_{\text{eff}}T_0/2LI_0$)
ΔH_R	heat of reaction (J/mol)
γ_R	dimensionless activation energy (E/RT_0)
ε_0	free space permittivity (Farad/m)
k'_{eff}	effective dielectric constant of packed bed
k''_{eff}	effective dielectric loss of packed bed
λ_{eff}	effective wavelength of microwave within packed column, m
λ_0	wavelength within free space, m
τ	dimensionless time
τ_D	diffusion number ($\phi\alpha_{\text{eff}}/D_{\text{eff}}$)
$\tau_{f_{\text{MW}}}$	dimensionless reaction time under microwave heating
$\tau_{f_{\text{Conv}}}$	dimensionless reaction time under conventional heating
θ	dimensionless temperature ($k_{\text{eff}}(T{-}T_0)/2LI_0$)
ϕ	porosity
Φ_R	bulk Thiele modulus ($4L^2\phi R(C_{A0}, T_0)/D_{\text{eff}}C_{A0}$)

the entire spectrum of microwave heating possibilities and their influence on overall progress of reaction.

Main objective of the current study is to fundamentally investigate the enhancement of reaction under various probable microwave heating scenarios (that can be encountered due to varying reactor dimension or dielectric properties of the reacting medium) and to show how the enhancement can be further improved by inserting a metallic coated surface at the other side of microwave incidence for certain specific cases. The reaction considered is a first order endothermic gas phase reaction occurring in a semiinfinite batch reactor in presence of susceptors. It may be noted that most of the common gases do not absorb microwave energy to significant extent and thus require susceptors to continue the reaction. Susceptors absorb microwave energy and transfer them to the gaseous reacting medium. Reactions can also be carried out without the help of susceptors in cases of microwave absorbing reacting medium e.g. dielectric liquid reactants. However, microwave propagation depends on reactant concentration within such system and change during the course of reaction depending on the specific material under consideration. Correspondingly, simulations of such microwave absorbing reacting system remain restricted to a specific material or a group of materials representing only a few specific microwave heating scenarios. This directed the current work to consider microwave non-absorbing gaseous reaction, which unleashes the limitations of material specific simulations and allows to perform a material invariant analysis considering all probable microwave propagation scenarios. Nevertheless, the results presented here can be extended for qualitative estimates of microwave absorbing liquid phase reactions.

The analysis is carried out via simulating progress of reaction from detailed mass and energy balance equations in conjunction with Helmholtz equation for microwave propagation. Simulations are carried out for microwave propagation with or without metal coated bounding surface in order to investigate the changes in reactor dynamics and probable enhancement of energy savings. Simulations are also carried out for reactions under equivalent conventional heating to quantify enhancement of reaction rate and corresponding reduction of energy consumption under microwave radiation in various probable scenarios of varying reactor dimensions, presence of metallic coated bounding surface, changing susceptor properties, varying reaction rate etc.

2. Mathematical modeling

The reacting system under consideration is a semiinfinite batch reactor as shown in Fig. 1, where the entrapped gas undergoes a first order endothermic conversion given by $A(g) \xrightarrow{k_R} B(g)$. This work considers two possible configurations of heating the reactor via microwave as shown in Fig. 1(a) and (b). The right wall of the reactor is coated with a reflective (metallic) material in subplot (a), while the reactor does not contain any reflective coating in subplot (b). The reflective material completely reflects back the microwave and hence alters the resulting heating pattern in the former compared to the later. In both the cases, the reactor is exposed to microwave of intensity I_0 from the left end and packed with highly microwave absorbing materials or susceptors (e.g. SiC). Note that susceptors are required since gaseous species do not absorb microwave in general and thus cannot be heated under microwave radiation by themselves. The two configurations with and without reflective coating will be referred as "type 1" and "type 2" reactors, respectively. To compare the efficiencies of the two microwave heating strategies, their equivalent conventional heating with same heating rate are also considered as shown in Fig. 1(c). It may be noted that intensities of conventional heating corresponding to type 1 and type 2 configurations may differ from each other due to changes in microwave propagation.

It is assumed that the reaction occurs only in the gas phase and the packing materials do not absorb any species. It is also assumed that material properties remain constant throughout the reaction, packings are homogenous and reactor walls are impermeable and thermally insulated. With further assumption of local thermal equilibrium and negligible convection in gas phase, evolution of reactant concentration (c_A) and temperature (T) from the uniform initial state of $C_{A,0}$ and T_0, respectively can be simulated from

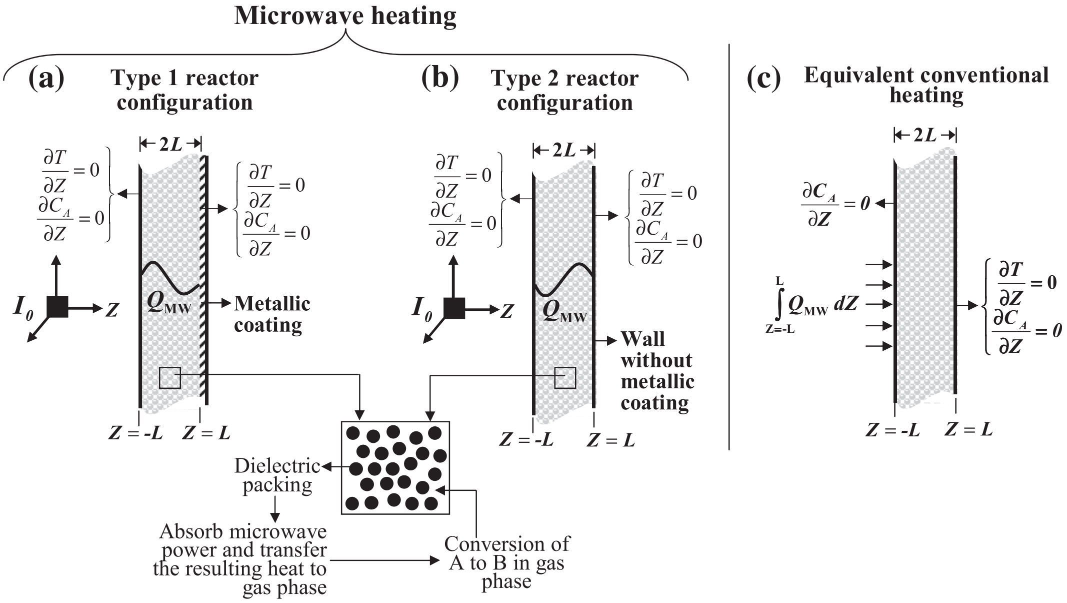
Microwave heating
(a) Type 1 reactor configuration
(b) Type 2 reactor configuration
(c) Equivalent conventional heating
2L
$\frac{\partial T}{\partial Z}=0$
$\frac{\partial C_A}{\partial Z}=0$
I_0
Z
Q_{MW}
Metallic coating
Wall without metallic coating
Z = -L
Z = L
$\int_{Z=-L}^{L} Q_{MW}\, dZ$
Dielectric packing
Absorb microwave power and transfer the resulting heat to gas phase
Conversion of A to B in gas phase

Fig. 1. Schematic representation of (a) type 1 and (b) type 2 reactor configurations (with and without metallic coating, respectively) under microwave heating with subplot (c) showing equivalent reactor configuration for conventional heating.

following mass and energy balance equations and the associated boundary conditions:

$$\phi\frac{\partial C_A}{\partial t} = D_{\text{eff}}\frac{\partial^2 C_A}{\partial Z^2} - \phi R(C_A,T) \tag{1a}$$

$$(\rho C_p)_{\text{eff}}\frac{\partial T}{\partial t} - k_{\text{eff}}\frac{\partial^2 T}{\partial Z^2} + \phi\Delta H_R R(C_A,T) = \begin{cases} Q_{\text{MW}} & \text{Microwave} \\ 0 & \text{Conventional} \end{cases} \tag{1b}$$

$$@Z = -L: \frac{\partial C_A}{\partial Z} = 0, \begin{cases} \frac{\partial T}{\partial Z} = 0 & \text{Microwave} \\ -k_{\text{eff}}\frac{\partial T}{\partial Z} = \int\limits_{-L}^{L} Q_{\text{MW}}dZ & \text{Conventional} \end{cases}, \tag{1c}$$

$$@Z = L: \frac{\partial C_A}{\partial Z} = 0, \frac{\partial T}{\partial Z} = 0. \tag{1d}$$

These equations have to be solved in conjunction with Helmholtz equation for electric field (E_m) along with radiation boundary conditions for scattering of waves at reactor boundaries given in Appendix A (see Eqs. (A.1)–(A.6) for evaluation of absorbed power distribution within type 1 and type 2 reactors (Q_{MW}) given by

$$Q_{\text{MW}} = \frac{2I_0\lambda_0}{\lambda_{\text{eff}}D_{p_{\text{eff}}}}\left(\frac{E_m}{E_0}\right)\left(\frac{E_m^*}{E_0}\right), \tag{2}$$

where E_m^* is the complex conjugate of E_m, λ_0 and λ_{eff} are wavelength of microwave with free space and reaction domain, respectively, $D_{p_{\text{eff}}}$ is the penetration depth of microwave within reaction domain and E_0 is the incident field (see Appendix A). Other variables used in Eqs. (1a)–(1d) are $2L$ as the reactor width, ϕ as porosity of packing, $D_{\text{eff}} = D_A\phi/\tau_p$, $(\rho C_p)_{\text{eff}} = \phi(\rho C_p)_g + (1-\phi)(\rho C_p)_p$ and $k_{\text{eff}} = \phi k_g + (1-\phi)k_p$ as effective diffusivity of reactant, effective heat capacity and effective thermal conductivity of the packed reaction domain, respectively, where subscripts g and p represent gas phase and packing material, respectively and D_A and τ_p are molecular diffusivity of species A and tortuosity of packing, respectively. In addition, ΔH_R is the heat of reaction and $R(C_A,T)$ is the first order reaction rate satisfying Arrhenius temperature dependency given by

$$R(C_A,T) = k_R C_A \exp\left[-\frac{E}{RT}\right], \tag{3}$$

where k_R is the first order rate constant, E is the activation energy and R is the universal gas constant.

In terms of the following dimensionless variables

$$z = \frac{Z+L}{2L}, \tau = \frac{\alpha_{\text{eff}}t}{4L^2}, \theta = \frac{k_{\text{eff}}(T-T_0)}{2LI_0},$$

$$c_A = \frac{C_A}{C_{A_0}}, q_{\text{MW}} = \frac{2LQ_{\text{MW}}}{I_0}$$

$$\tilde{E}_m = \frac{E_m}{E_0}, r(c_A,\theta) = \frac{R(C_A,T)}{R(C_{A_0},T_0)}, \gamma_R = \frac{E}{RT_0}, \tag{4}$$

where $\alpha_{\text{eff}} = k_{\text{eff}}/(\rho C_p)_{\text{eff}}$ is the effective thermal diffusivity of the packed reaction domain, dimensionless form of governing mass balance, energy balance and Helmholtz equation and their associated boundary conditions (Eqs. (1a)–(1d) and Eqs. (A.1), (A.4) and (A.5a), (A.5b)) can be rewritten as

$$\tau_D\frac{\partial c_A}{\partial \tau} = \frac{\partial^2 c_A}{\partial z^2} - \Phi_R r(c_A,\theta), \tag{5a}$$

$$\frac{\partial \theta}{\partial \tau} - \frac{\partial^2 \theta}{\partial z^2} + N_R r(c_A,\theta) = \begin{cases} q_{\text{MW}} & \text{Microwave} \\ 0 & \text{Conventional} \end{cases}, \tag{5b}$$

$$\frac{d^2\tilde{E}_m}{dz^2} + 4\pi^2 N_w^2\left(1+if_p\right)^2\tilde{E}_m = 0, \tag{5c}$$

$$@z = 0 : \begin{cases} \dfrac{\partial c_A}{\partial z} = 0, -\dfrac{\partial \theta}{\partial z} = \begin{cases} 0 & \text{Microwave} \\ \overline{q}_{\mathrm{MW}} & \text{Conventional} \end{cases}, \\ \dfrac{1}{2\pi N_w f_w}\dfrac{\mathrm{d}\tilde{E}_m}{\mathrm{d}z} + i\tilde{E}_m = 2i\exp[-i\pi N_w f_w], \end{cases} \tag{5d}$$

$$@z = 1 : \begin{cases} \dfrac{\partial \theta}{\partial z} = \dfrac{\partial c_A}{\partial z} = 0, \\ \tilde{E}_m = \begin{cases} 0 & \text{Type 1} \\ -\dfrac{i}{2\pi N_w f_w}\dfrac{\mathrm{d}\tilde{E}_m}{\mathrm{d}z} & \text{Type 2} \end{cases}, \end{cases} \tag{5e}$$

supplemented with the following expressions for dimensionless reaction rate ($r(c_A,\theta)$) and dimensionless absorbed power (q_{MW})

$$r(c_A,\theta) = c_A \exp\left[\gamma_R \frac{\theta}{\theta+\beta}\right], q_{\mathrm{MW}} = \frac{4\pi N_w f_p}{f_w}\tilde{E}_m \tilde{E}_m^{\,*}, \tag{6}$$

where dimensionless heat flux for conventional heating given by $\overline{q}_{\mathrm{MW}} = \int_{z=0}^{1} q_{\mathrm{MW}}(z)\mathrm{d}z$ is the dimensionless average absorbed power under microwave radiation. In this formulation, dimensionless parameters N_w (wave number), f_p and f_w characterize wave propagation within the reactor and are defined as

$$N_w = \frac{2L}{\lambda_{\mathrm{eff}}}, f_p = \frac{\lambda_{\mathrm{eff}}}{2\pi D_{p_{\mathrm{eff}}}}, f_w = \frac{\lambda_{\mathrm{eff}}}{\lambda_0}, \tag{7}$$

where N_w captures the effect of reactor thickness on wave propagation and dimensionless parameters f_w and f_p capture the effect of dielectric properties on microwave induced heating. [It may be noted that the combination $2\pi N_w f_p = 2L/D_{p_{\mathrm{eff}}}$ is the measure of reactor thickness compared to the penetration depth of microwave and is called penetration number or N_p in literature [61,62,64]]. The other four dimensionless numbers given by Φ_R (bulk Thiele modulus), τ_D (diffusion number or Lewis number), N_R (heat-reaction number) and β (conduction number) quantify relative magnitudes of various reaction and transport time scales within the reactor and are defined as

$$\Phi_R = \frac{t_D}{t_R}, \beta = \frac{t_H}{t_\alpha}, \tau_D = \frac{\phi t_D}{t_\alpha}, N_R = \frac{t_H}{t_{\Delta H_R}}, \tag{8}$$

where $t_D = 4L^2/D_{\mathrm{eff}}$, $t_\alpha = 4L^2/\alpha_{\mathrm{eff}}$, $t_R = C_{A_0}/\phi R(C_{A_0},T_0)$, $t_{\Delta H_R} = ((\rho C_p)_{\mathrm{eff}}T_0)/(\phi \Delta H_R R(C_{A_0},T_0))$ and $t_H = (2L(\rho C_p)_{\mathrm{eff}}T_0)/I_0$ represent mass diffusion time, thermal diffusion time, reaction time, cooling time due to heat absorption by reaction and heating time, respectively. It may be noted that Φ_R and β capture mass and heat transport resistances within the reactor, respectively, N_R measures relative supply of heat compared that required by reaction and τ_D quantifies relative speed of mass and thermal diffusion within the reactor.

3. Solution technique

The governing equations (Eq. (5)) are spatially discretized via weak formulation of Galerkin finite element method using 50 quadratic elements and time integrated using Crank-Nicholson scheme with a time step of $\Delta\tau = 10^{-4}$. The resulting nonlinear algebraic equations are solved at each time step by Newton–Raphson method following the same procedure as laid out in an earlier article [74]. It is worthwhile to mention here that simulation of endothermic reaction requires to stop the reaction locally and temporarily wherever and whenever local temperature reduces below a critical level (say T_{crit} or θ_{crit} in dimensionless scale). This is to avoid unrealistic temperature drop during the simulation due to absorption of heat by reaction especially in no/low heating zones within the reactor. Reaction is resumed back once local temperature increases to T_{crit}. This causes the reaction rate to undergo a step jump given by

$$r(c_A,\theta) = \begin{cases} c_A \exp\left[\gamma_R \dfrac{\theta}{\theta+\beta}\right] & \text{for } \theta \geq \theta_{\mathrm{crit}} \\ 0 & \text{otherwise} \end{cases}, \tag{9}$$

which causes the tracing of its dynamics to be numerically challenging due to introduction of Dirac delta function in the Jacobian matrix [75]. However, following the suggestion of an earlier work on tracing the phase change of pure materials [75], the numerical difficulties are efficiently circumvented by smoothing the step jump with a linear function within a superficial reaction zone of width $2\Delta T$ around T_{crit} as shown in Fig. 2. The modified rate expression with inclusion of superficial reaction zone can be written in terms of dimensionless variables as

$$\hat{r}(c_A,\theta) = \begin{cases} 0 & \text{for } \theta \leq \theta_{crit} - \varepsilon \\ r(c_A,\theta_{crit}+\varepsilon)\left[\dfrac{\theta - \theta_{crit} + \varepsilon}{2\varepsilon}\right] & \text{for } \theta_{crit} - \varepsilon \leq \theta \leq \theta_{crit} + \varepsilon, \\ r(c_A,\theta) & \text{for } \theta > \theta_{crit} + \varepsilon \end{cases} \tag{10}$$

where $\varepsilon = k_{\mathrm{eff}}\Delta T/2LI_0$ is half width of the superficial reaction zone in dimensionless temperature scale. Convergence of numerical simulations with respect to the width of superficial reaction zone are shown in Fig. 3, which shows variations of overall reactant depletion rate $(1-\overline{c}_A)$ as ε is varied from 10^{-3} to 10^{-6} (dotted, dash and solid lines and circles). Simulations in Fig. 3 are carried out for low intensity conventional heating corresponding to type 1 and type 2 configurations at $N_w = 0.06$, $f_w = 0.1$, $f_p = 0.1$ ($\overline{q}_{\mathrm{MW}} = 0.002$ and 0.141, respectively). It may be noted that unrealistic temperature drop during the simulation become more probable for surface heating (at regions far away from heat source) than volumetric heating of microwave especially for low intensity of $\overline{q}_{\mathrm{MW}}$. As a result, simulations require much frequent use of superficial reaction zone (Eq. (10)) in cases of low intensity of conventional heating. Correspondingly, convergence of numerical simulations in the two severe cases presented in Fig. 3 guarantees convergence for all other cases. Other parameters in Fig. 3 correspond to $\Phi_R = 10$, $\tau_D = 1$, $N_R = 0.1$, $\beta = 0.1$ and $\gamma_R = 10$. Fig. 3 shows that numerical simulations become invariant of the width of superficial reaction

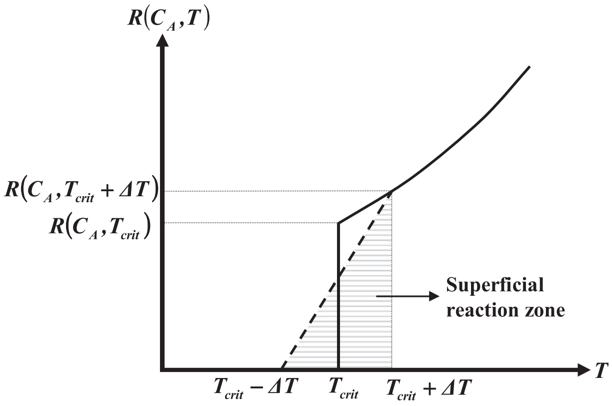

Fig. 2. Schematic representation of superficial reaction zone.

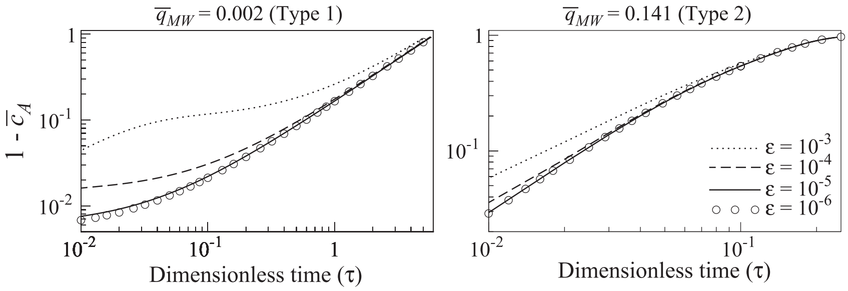

Fig. 3. Convergence of numerical simulation with respect to the width of superficial reaction zone (ε) shown in terms of $1-\overline{c}_A$vs τ at $\varepsilon = 10^{-3}$ (dotted lines), 10^{-4} (dashed lines), 10^{-5} (solid lines) and 10^{-6} (circles) for two severe cases of slow surface heating corresponding to type 1 and type 2 configurations at $N_w = 0.06$, $f_p = 0.1$ and $f_w = 0.1$ with $\overline{q}_{\text{MW}} = 0.002$ and 0.141, respectively with other parameters as $\tau_D = 1$, $N_R = 0.1$, $\beta = 0.1$, $\Phi_R = 10$ and $\gamma_R = 10$.

zone at $\varepsilon = 10^{-5}$ even for these severe situations. Hence, we will use $\varepsilon = 10^{-5}$ for all the simulations. It may be noted that we have assumed $T_{\text{crit}} = T_0$ in Fig. 3 and will use the same in all forthcoming illustrations.

Starting from $c_A = 1$ and $\theta = 0$ at $\tau = 0$, all simulations are stopped when conversion reaches 90% across the entire reactor corresponding to $\max(c_A) = 0.1$. Time required for this conversion will be referred as reaction time and denoted by $\tau_{f_{\text{MW}}}$ and $\tau_{f_{\text{Conv}}}$ for microwave and conventional heating, respectively. Simulations are carried out for different reactor dimensions over the entire range of N_w to replicate various possible microwave heating scenarios and their alteration due to metallic coating. For all the cases, reactor dynamics are simulated and compared for two limiting cases of weak and strong mass transfer limitations within the reactor via $\Phi_R = 0.1$ and 10, respectively with fixed relative heat supply as well as fixed heat transfer limitations at $N_R = 0.1$ and $\beta = 0.1$, respectively. It may be noted that $N_R \ll 1$ ensures enough heat supply to the reactor compared to the heat requirement for reaction. On the other hand, higher thermal diffusion time compared to heating time at $\beta \ll 1$ allows to simulate distinct dynamics of microwave and conventional heating [74]. It is important to note that heating of reactor becomes invariant of the supply pattern for $\beta \gg 1$, where supplied heat spreads uniformly across the reactor instantaneously. Other parameters are selected to be $\tau_D = 1$ (to avoid preferential diffusion of either heat of mass) and $\gamma_R = 10$.

4. Model validation

In absence of any appropriate experimental or numerical data in literature, we validate the present simulations by comparing them with the analytical solutions which can be obtained in the limit of $\gamma_R \to 0$. In this limit of $\gamma_R \to 0$, the nonlinear mass and energy balance equations (Eqs. (5a) and (5b)) reduce to the following linear ones:

$$\tau_D \frac{\partial c_A}{\partial \tau} = \frac{\partial^2 c_A}{\partial z^2} - \Phi_R c_A, \tag{11a}$$

$$\frac{\partial \theta}{\partial \tau} - \frac{\partial^2 \theta}{\partial z^2} + N_R c_A = \begin{cases} q_{\text{MW}} & \text{Microwave} \\ 0 & \text{Conventional} \end{cases}, \tag{11b}$$

along with the boundary conditions given by Eqs. (5d) and (5e) and the initial conditions given by $c_A = 1$ and $\theta = 0$ at $\tau = 0$. Using Finite Fourier Transformations (FFT), closed form solutions of the above equations are obtained as

$$c_A(\tau) = \exp\left[-\frac{\Phi_R}{\tau_D}\tau\right], \tag{12a}$$

$$\theta(z,\tau) = \tau\overline{q}_{\text{MW}} - \frac{N_R \tau_D}{\Phi_R}\left(1 - \exp\left[-\frac{\Phi_R}{\tau_D}\tau\right]\right) + \sum_{n=1}^{\infty} \frac{1-\exp[-\lambda_n \tau]}{\lambda_n} w_n(z) \begin{cases} \langle q_{\text{MW}}, w_n\rangle & \text{Microwave} \\ \sqrt{2}\overline{q}_{\text{MW}} & \text{Conventional}, \end{cases} \tag{12b}$$

where $\lambda_n = n^2\pi^2$ is the nth eigenvalue, $w_n(z)$ is the nth eigenfunction given by

$$w_n(z) = \begin{cases} 1 & n = 0 \\ \sqrt{2}\cos n\pi z & n \geq 1 \end{cases}, \tag{12c}$$

and $\langle q_{\text{MW}}, w_n\rangle$ is the inner product defined as

$$\langle q_{\text{MW}}, w_n\rangle = \int_{z=0}^{1} q_{\text{MW}}(z) w_n(z) \mathrm{d}z. \tag{12d}$$

The expressions for $\langle q_{\text{MW}}, w_n\rangle$ and $\overline{q}_{\text{MW}}$ are given in Appendix B (Eqs. (B.4) and (B.5)).

To compare numerical results, reactor dynamics in the limit of $\gamma_R \to 0$ are simulated from Eq. (5) by using $\gamma_R = 0.001$ with other parameters as $\Phi_R = 10$, $N_R = 0.1$, $\tau_D = 1.0$ and $\beta = 0.1$ (same as in Fig. 3). Resulting concentration and temperature profiles are compared with those obtained from the analytical expressions (Eqs. (12a) and (12b), respectively) for three different reactor dimensions of $N_w = 0.25$, 0.5 and 0.75 with $f_p = 0.1$ and $f_w = 0.1$ as shown in Fig. 4(a)–(b). These three reactor dimensions correspond to various probable stiffness of microwave heating patterns (as reflected in the corresponding temperature profiles) and also correspond to a wide range of conventional heating intensities ($\overline{q}_{\text{MW}} = 0.949$, 0.114 and 0.6 for type 1 configuration and $\overline{q}_{\text{MW}} = 0.059$, 0.504 and 0.158, for type 2 configuration at $N_w = 0.25$, 0.5 and 0.75, respectively). Fig. 4 shows the comparisons for both microwave (MW) and conventional (Conv.) heatings, where bullets represent numerical simulations and continuous lines represent analytical solutions with darker and lighter shades indicating type 1 and type 2 configurations, respectively. The spatial profiles in Fig. 4 are shown at $\tau = 0.15$, which is half the time required for completion of 90% conversion [Note: analytical solution predicts required reaction time as $\tau = 0.2303$, while simulations predict required reaction time to be $\tau = 0.2307$]. It may be noted that in the limit of $\gamma_R \to 0$, reactant concentration and its consumption becomes invariant of heating mode and hence invariant of spatial location within the reactor (as reflected in Eq. (12a)). Accordingly, numerical simulations predict uniform concentration for both microwave and conventional heating irrespective of reactor dimension as shown in Fig. 4(a). In contrast to concentration, temperature

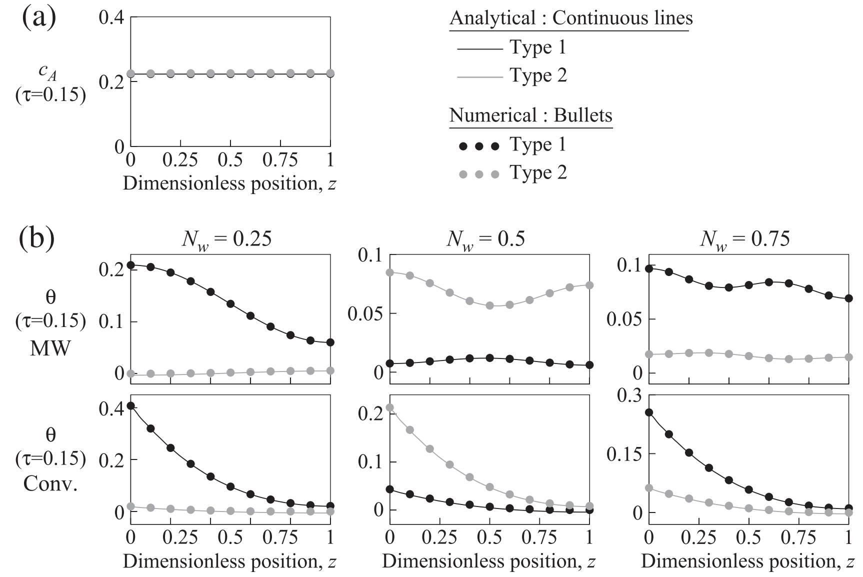

Fig. 4. Comparison between simulated results (bullets) and analytical solutions (continuous lines) for type 1 and type 2 configurations (represented by darker and lighter shades, respectively) in case of three representative reactor dimensions of $N_w = 0.25$, 0.5 and 0.75 with $f_p = 0.1$, $f_w = 0.1$, $N_R = 0.1$, $\tau_D = 1$, $\Phi_R = 10$, $\beta = 0.1$ and $\gamma_R = 0.001$. Subplot (a) shows comparison of concentration profiles at $\tau = 0.15$ and subplot (b) shows comparison of temperature profiles for microwave heating (MW) and corresponding conventional heating (Conv.) at $\tau = 0.15$.

profiles depend on heating patterns and thus vary with heating mode, reactor configuration and reactor dimension as shown in Fig. 4(b). Nevertheless, numerical simulations are in excellent agreement with analytical solutions in all the cases showing the accuracy of the solutions for different probable heating scenarios.

5. Microwave power absorption and influence of metallic coating

Influence of metallic coating on microwave power absorption are measured by two factors: (i) changes in the spatial distribution of absorbed power (q_{MW}) and (ii) variations in the intensity of $\overline{q}_{\mathrm{MW}}$ or surface heat flux. Spatial distribution of absorbed power determines the homogeneity of microwave heating, which in conjunction with intensity of conventional heating ($\overline{q}_{\mathrm{MW}}$) play a critical role in determining the efficiency of microwave heating. Influence of metallic coating on the above two factors are shown in Fig. 5, where the main plot shows the variations of $\overline{q}_{\mathrm{MW}}$ and the representative insets show the variations of absorbed power distributions from type 1 (solid lines) to type 2 (dotted lines) configurations for various probable microwave heating scenarios spanning the range of reactor dimension given by $0.05 \le N_w \le 10$. The results in Fig. 5 are simulated using $f_p = 0.1$ and $f_w = 0.1$.

The insets of Fig. 5 show that entire spectrum of power absorption patterns can be categorized in three distinct classes of *uniform* ($N_w = 0.06$), (ii) *oscillatory* ($N_w = 0.5$ and 0.75) and (iii) *exponentially attenuated* ($N_p = 3$) profiles. These three patterns appear in chronological order as reactor dimension increases from much below the wavelength of microwave ($N_w \le 0.1$) to much greater than penetration depth of microwave ($N_p \ge 3$) and divide the entire range of reactor dimensions in *thin* ($N_w \le 0.1$), *intermediate* ($0.1 < N_w$ and $N_p < 3$) and (iii) *thick* ($N_p \ge 3$) regimes, respectively [62]. *Thin* regime refers to the entire range of reactor dimensions below $N_w = 0.1$, where microwave power absorption occurs uniformly irrespective of metallic coating as seen in the inset for $N_w = 0.06$. However, metallic coating significantly reduces microwave power absorption in *thin* regime as can be seen from the magnitudes of $\overline{q}_{\mathrm{MW}}$ for $N_w \le 0.1$ in Fig. 5. It may be noted that microwave power absorption in type 1 configuration becomes insignificantly small as N_w decreases beyond 0.05.

Thick regime refers to the reactors with dimensions much greater than penetration depth of microwave ($N_p \ge 3$), where microwave losses most its energy before reaching the other end of the reactor. Correspondingly, power absorption in *thick* regime occurs only near the exposed surface and remain unaltered by the presence of metallic coating as seen in Fig. 5 for $N_p \ge 3$. It may be seen from the inset for $N_p = 3$ that absorbed power attenuates exponentially from the exposed surface in *thick* regime. Power absorption regime further shrinks with increasing reactor dimension and microwave heating approaches surface heating in the limit of $N_p \to \infty$.

Intermediate regime refers to the reactors in between *thin* and *thick* regimes ($0.1 < N_w < 3/2\pi f_p$), where reactor dimensions are neither much lower than wavelength of microwave nor much greater than penetration depth of microwave. In this regime, microwave power absorption is strongly dependent on the nature of scattering from the reactor walls. Scattering of microwaves form various traveling waves within the reactor and interferences between them determine the resultant power absorption characteristics depending on phase-space of individual wave [62]. Since metallic coating alters scattering by completely reflecting microwaves from the right wall, resulting traveling waves in type 1 configuration also differ significantly from those in type 2 configuration. As a result, *intermediate* regime exhibits most prominent influence of metallic coating as seen in Fig. 5.

Most important characteristic of *intermediate* regime is the oscillatory variations of $\overline{q}_{\mathrm{MW}}$ with reactor dimension, which result from constructive and destructive interferences between traveling waves. Constructive interference enhances power absorption, while destructive interference suppresses power absorption. In *intermediate* regime, constructive interferences occur at periodic intervals as reactor dimension increases from 0.1 to $3/2\pi f_p$ and every two consecutive constructive interferences are accompanied by a destructive interference in between [62]. Hence, $\overline{q}_{\mathrm{MW}}$ undergoes periodic enhancement and suppression over the range of *intermediate* regime, which is reflected in Fig. 5 as a series of

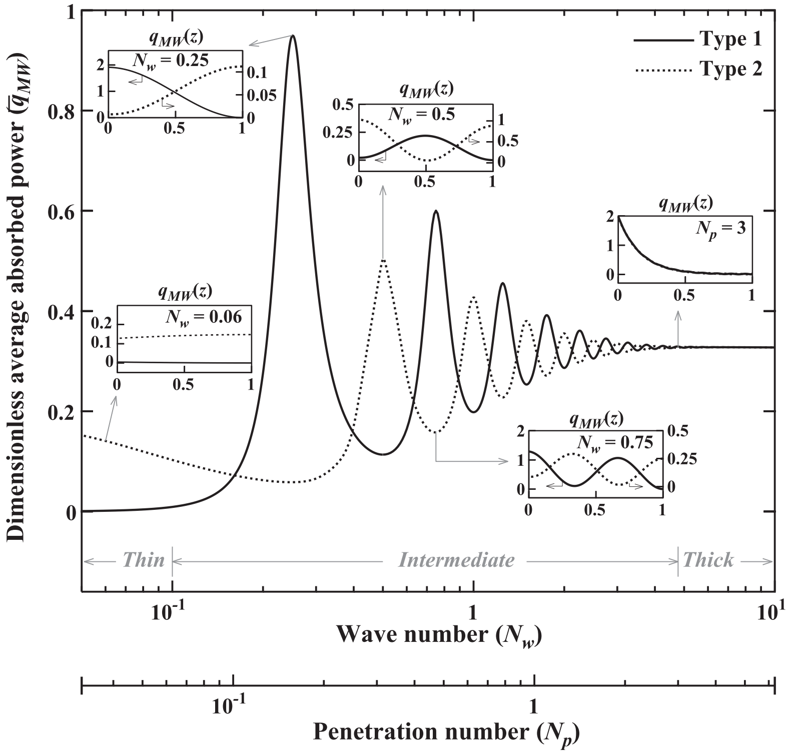

Fig. 5. Influence of metallic coating on $\overline{q}_{MW}$ over the entire range of *thin* to *thick* regimes ($0.05 \le N_w \le 10$) as well as influence of metallic coating on the power absorption profiles [$q_{MW}(z)$] at representative reactor dimensions (N_w or N_p), where solid and dotted lines represent reactors with (type 1) and without (type 2) metallic coating, respectively and parameters f_w and f_p are taken to be 0.1.

maxima and minima of $\overline{q}_{MW}$ for both type 1 and type 2 reactors. Enhancement of $\overline{q}_{MW}$ at locations of its maxima are also called resonances. Fig. 5 shows that locations of resonances depend strongly on reactor configuration, where resonances for type 1 configuration occur at the locations of minima for type 2 configuration and vice versa. Resonances occur at $N_w = 0.5n$, $n = 1,2\ldots$ for type 2 configuration, where type 1 configuration leads to minima of $\overline{q}_{MW}$. Similarly, resonances for type 1 configuration occur at $N_w = 0.5n-0.25$, $n = 1,2\ldots$, where $\overline{q}_{MW}$ exhibits minima for type 2 configuration (see Fig. 5). Amplitudes of resonances are also much higher in type 1 configuration than type 2.

Similar to $\overline{q}_{MW}$, power absorption patterns of *intermediate* regime are also strongly influenced by metallic coating, where type 1 and type 2 configurations lead to completely opposite absorbed power distributions as illustrated in Fig. 5 for $N_w = 0.25$, 0.5 and 0.75. Typical feature of *intermediate* regime is the presence of local maxima in absorbed power distributions due to occurrence of spatial resonances, where larger reactor favors more spatial resonances as can be seen from the insets of Fig. 5 for $N_w = 0.25$, 0.5 and 0.75. In all the cases, locations of spatial maxima in type 1 configuration correspond to locations of local minima of absorbed power in type 2 configuration and vice versa.

6. Alteration of reactor dynamics under microwave heating and influence of metallic coating

Alteration of reactor dynamics under *thin*, *intermediate* and *thick* regimes of microwave heating for type 1 and type 2 configurations are illustrated in Figs. 6–10 for the representative reactor dimensions corresponding to $N_w = 0.06$ (Fig. 6), 0.25 (Fig. 7), 0.5 (Fig. 8), 0.75 (Fig. 9) and $N_p = 3$ (Fig. 10). In each case, influences of microwave heating are illustrated for two limiting cases of weak and strong mass transfer limitations at $\Phi_R = 0.1$ and 10 in subplots (a) and (b), respectively. It may be noted that reactor dynamics under microwave heating are shown at the top panel in each subplot of Figs. 6–10 and are denoted by “MW”. Reactor dynamics under conventional heating corresponding to type 1 and type 2 configurations of various N_w’s and N_p are shown at the bottom panel in each subplot of Figs. 6–10 and are denoted by “Conv”. In all the cases, parameters f_p and f_w are considered to be 0.1 and type 1 and type 2 configurations are represented by solid and dashed lines, respectively. Here, reactor dynamics are compared in terms of spatial non-uniformities of reaction pattern ($N_R r(c_A,\theta$ vs $z)$ and reactant concentration (c_A vs z) within the reactor as well as overall reactant depletion rate ($\overline{c}_A$vs τ). In each figure, spatial non-uniformities within the reactor are shown at two intermediate time levels given by $\tau_f/3$ (darker shade) and $2\tau_f/3$ (lighter shade). Power absorption profiles along with magnitude of $\overline{q}_{MW}$ for type 1 and type 2 reactor configurations of Figs. 6–10 are also shown at top of each figure for ease of illustrations.

Alteration of reaction dynamics under microwave heating is purely driven by individual power absorption patterns of type 1 and type 2 configurations in *thin*, *intermediate* and *thick* regimes. Conventional or surface heating always results in localized reaction from the hot left surface, where intensity of reaction is purely determined by the surface heat flux or $\overline{q}_{MW}$. On the other hand, reaction occurs volumetrically under microwave heating but with varying spatial profiles depending on the regime of operation and reactor configuration. Reaction occurs uniformly under *thin* regime of microwave heating ($N_w \le 0.1$) as reflected in almost uniform spatial profiles of $N_R r(c_A,\theta)$ at $N_w = 0.06$ for both type 1 and type 2 configurations. In contrast, reaction occurs only near the exposed left surface (similar to conventional heating) in *thick* regime of microwave heating as seen in the spatial profiles of $N_R r(c_A,\theta)$ for $N_p = 3$ in Fig. 10. In between these two regimes, reaction patterns under microwave heating vary with reactor dimension as well as

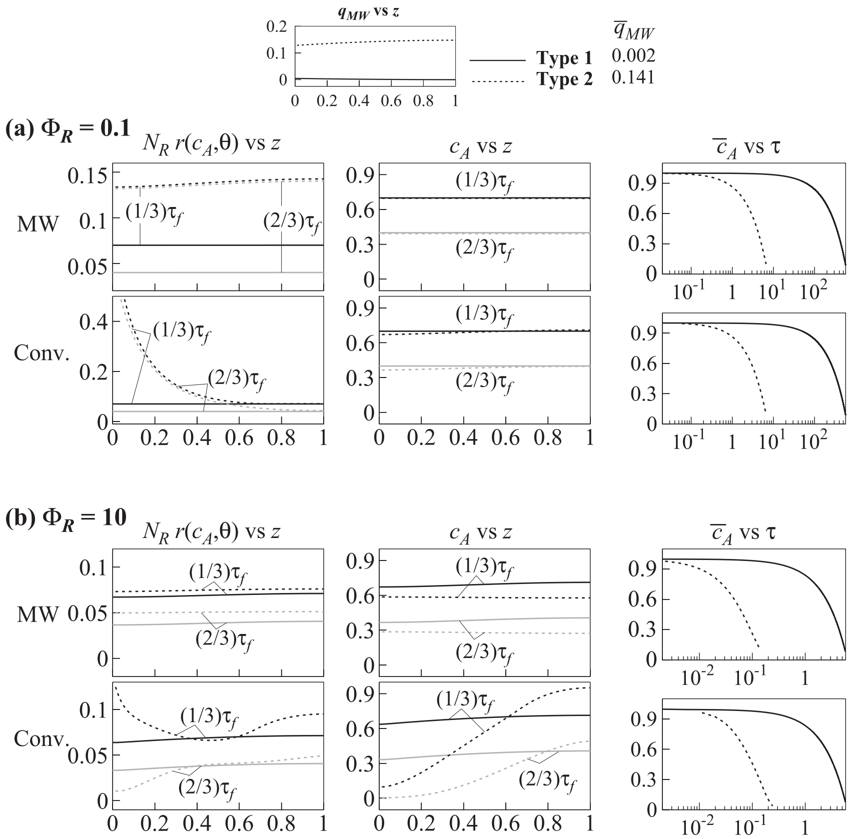

Fig. 6. Spatial dynamics ($N_R r(c_A,\theta)$ vs z and c_A vs z shown at $\tau_f/3$ and $2\tau_f/3$ in darker and lighter shades, respectively) and overall progress ($\overline{c}_A$vs τ) of type 1 (solid lines) and type 2 (dotted lines) reactors under microwave heating (MW) along with those under their equivalent convectional heating (Conv.) in *thin* regime corresponding to $N_w = 0.06, f_w = 0.1$ and $f_p = 0.1$ with $\tau_D = 1.0$, $N_R = 0.1$, $\beta = 0.1$, $\gamma_R = 10$ and $\Phi_R = 0.1$ and 10 in subplots (a) and (b), respectively.

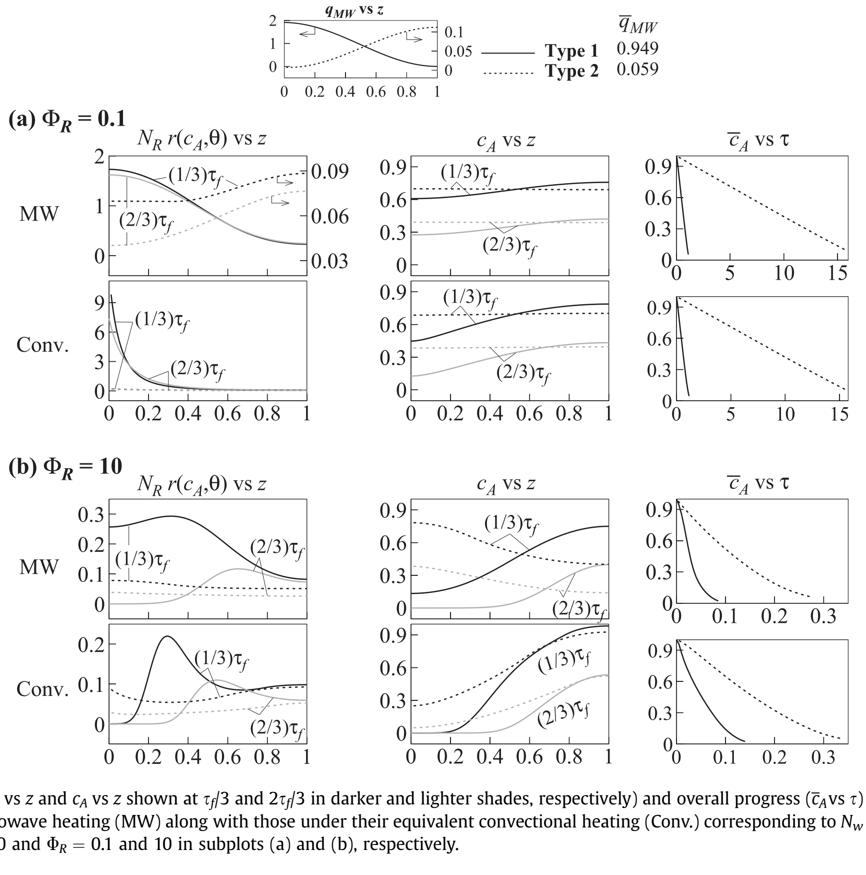

Fig. 7. Spatial dynamics ($N_R r(c_A,\theta)$ vs z and c_A vs z shown at $\tau_f/3$ and $2\tau_f/3$ in darker and lighter shades, respectively) and overall progress ($\overline{c}_A$vs τ) of type 1 (solid lines) and type 2 (dotted lines) reactors under microwave heating (MW) along with those under their equivalent convectional heating (Conv.) corresponding to $N_w = 0.25, f_w = 0.1$ and $f_p = 0.1$ with $\tau_D = 1.0$, $N_R = 0.1$, $\beta = 0.1$, $\gamma_R = 10$ and $\Phi_R = 0.1$ and 10 in subplots (a) and (b), respectively.

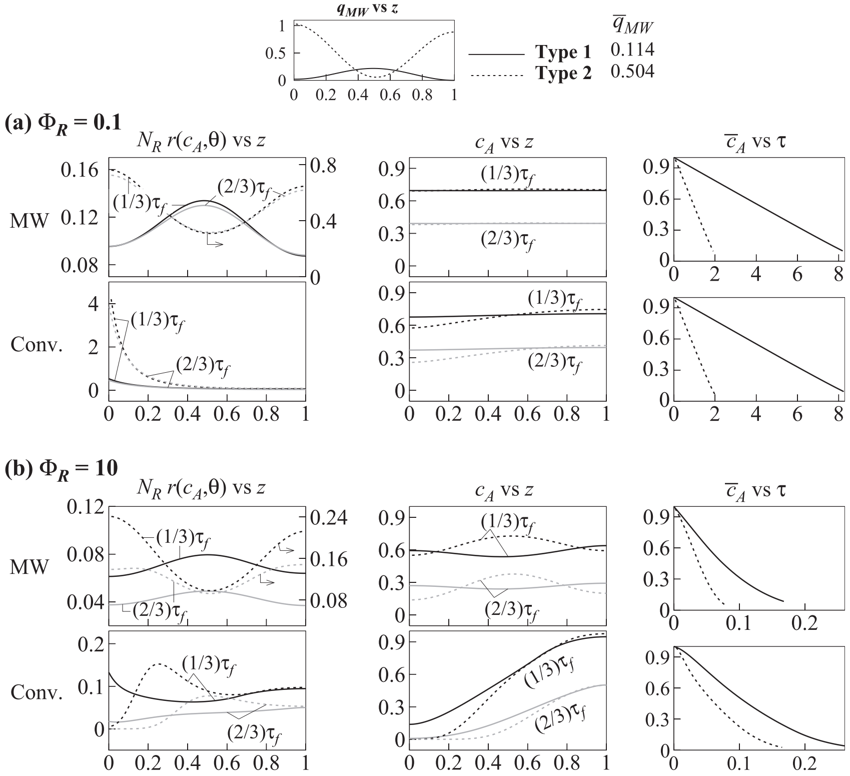

Fig. 8. Spatial dynamics [$N_R r(c_A,\theta)$ vs z and c_A vs z shown at $\tau_f/3$ and $2\tau_f/3$ in darker and lighter shades, respectively] and overall progress [$\overline{c}_A$vs τ] of type 1 (solid lines) and type 2 (dotted lines) reactors under microwave heating (MW) along with those under their equivalent convectional heating (Conv.) in *intermediate* regime corresponding to $N_w = 0.5$, $f_w = 0.1$ and $f_p = 0.1$ with $\tau_D = 1.0$, $N_R = 0.1$, $\beta = 0.1$, $\gamma_R = 10$ and $\Phi_R = 0.1$ and 10 in subplots (a) and (b), respectively.

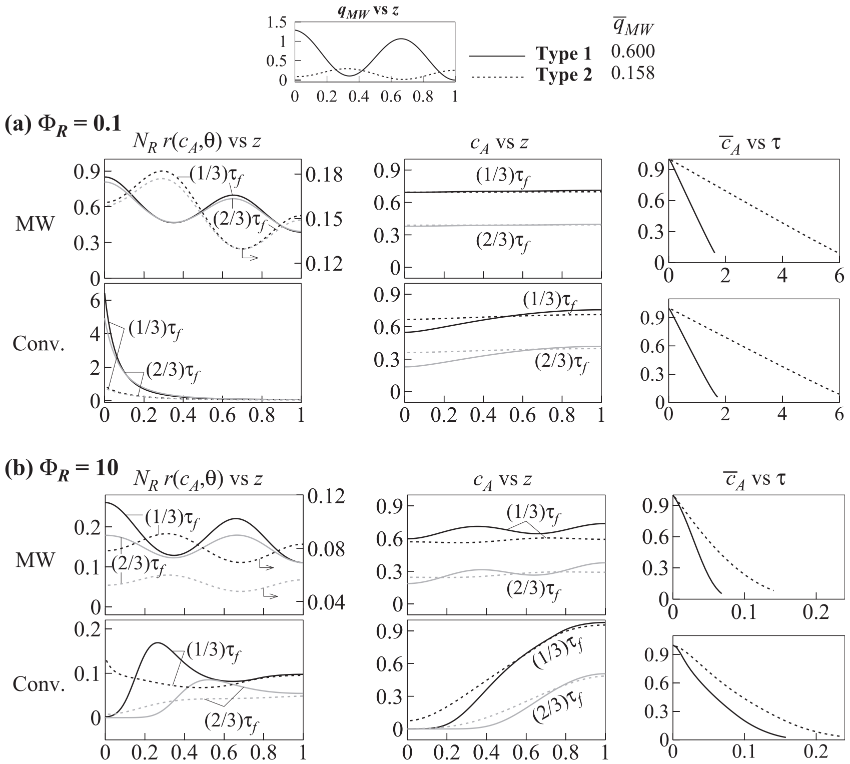

Fig. 9. Spatial dynamics ($N_R r(c_A,\theta)$ vs z and c_A vs z shown at $\tau_f/3$ and $2\tau_f/3$ in darker and lighter shades, respectively) and overall progress ($\overline{c}_A$vs τ) of type 1 (solid lines) and type 2 (dotted lines) reactors under microwave heating (MW) along with those under their equivalent convectional heating (Conv.) in *intermediate* regime corresponding to $N_w = 0.75$, $f_w = 0.1$ and $f_p = 0.1$ with $\tau_D = 1.0$, $N_R = 0.1$, $\beta = 0.1$, $\gamma_R = 10$ and $\Phi_R = 0.1$ and 10 in subplots (a) and (b), respectively.

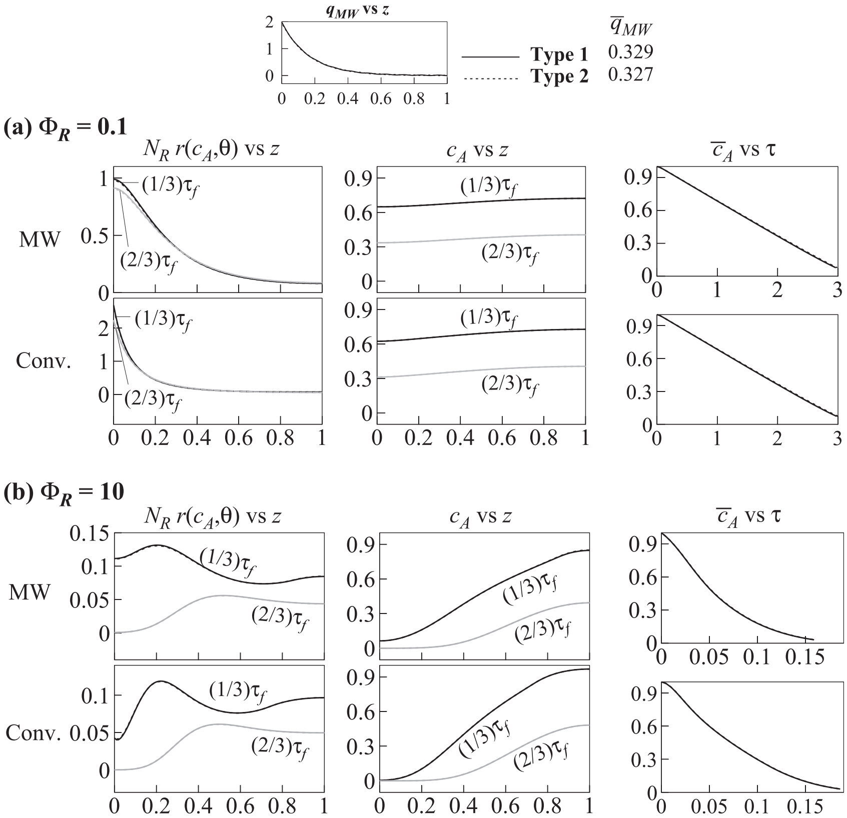

Fig. 10. Spatial dynamics ($N_R r(c_A,\theta)$ vs z and c_A vs z shown at $\tau_f/3$ and $2\tau_f/3$ in darker and lighter shades, respectively) and overall progress ($\overline{c}_A$ vs τ) of type 1 (solid lines) and type 2 (dotted lines) reactors under microwave heating (MW) along with those under their equivalent convectional heating (Conv.) in *thick* regime corresponding to $N_p = 3$, $f_w = 0.1$ and $f_p = 0.1$ with $\tau_D = 1.0$, $N_R = 0.1$, $\beta = 0.1$, $\gamma_R = 10$ and $\Phi_R = 0.1$ and 10 in subplots (a) and (b), respectively.

configuration but remain bound within uniform reaction of *thin* regime and surface reaction of *thick* regime. Reactions mostly occur volumetrically under *intermediate* regime of microwave heating except near the boundaries of *thin* and *thick* regimes. It is interesting to note that similar to *thick* regime, reaction under microwave heating also becomes highly one sided within a small region near the boundary of *thin* regime around $N_w \approx 0.25$, where reaction is driven from the reactor boundary as seen in Fig. 7 for $N_w = 0.25$.

Special characteristics of reaction under *intermediate* regime of microwave heating is presence of multiple reaction fronts at the locations of spatial resonances especially for larger reactors ($N_w \geq 0.5$). Reactor with dimensions $N_w < 0.5$ leads to a single reaction front irrespective of reactor configuration as seen in Fig. 7 for $N_w = 0.25$. However, location of reaction front changes from left to right surface as reactor configuration changes from type 1 to type 2 at $N_w = 0.25$ (see Fig. 7). Location of reaction front under microwave heating also changes from the center to both the surfaces as reactor configuration is changed from type 1 to type 2 at $N_w = 0.5$. This interestingly introduces two reaction fronts in type 2 configuration at $N_w = 0.5$ in contrast to the single reaction front in type 1 configuration (see Fig. 8). Reactors with $N_w \geq 0.75$ lead to multiple reaction fronts irrespective of reactor configurations, but reaction fronts of type 1 configuration always appear in the locations of minimum reaction zones of type 2 configuration as illustrated in Fig. 9 for $N_w = 0.75$.

Common feature of all the reaction patterns is homogeneity of reaction under microwave heating compared to their conventional counterparts except for very thick reactors with $N_p \to \infty$. Correspondingly, both type 1 and type 2 reactors exhibit homogenized concentration profiles under microwave heating in presence of mass transfer limitations at $\Phi_R = 10$ as illustrated in subplot (b) of Figs. 6–10. Mass transfer limitations exist when diffusion of reactant is slower than its consumption rate or equivalently $\Phi_R \gtrsim 1$. In such cases, reactant builds up in no/low reaction zones of the reactor according to the non-uniformity of reaction pattern. Volumetric power absorption significantly enhances the uniformity of reaction from conventional to microwave heating in *thin* and *intermediate* regimes (except around $N_w \approx 0.25$). As a result, reactors with $N_p < 3$ and $N_w \not\approx 0.25$ show prominent homogenization of concentration gradients under microwave heating compared to conventional heating as shown in Figs. 6(b), 8(b) and 9(b) for $N_w = 0.06$, 0.5 and 0.75, respectively. On the other hand, highly one sided reaction from the surface significantly reduces homogenization ability of microwave heating around $N_w \approx 0.25$ as well as in *thick* regime as illustrated in Figs. (7b) and (10b) for $N_w = 0.25$ and $N_p = 3$, respectively.

Homogenization ability of microwave heating also depends on the degree of localization in its conventional counterpart and thus on the intensity of $\overline{q}_{\mathrm{MW}}$. Reactor dynamics remain homogenized (uniform) even under conventional heating if intensity of $\overline{q}_{\mathrm{MW}}$ remains sufficiently low such that resulting spatial gradients can be easily homogenized by diffusion. For such low intensity of $\overline{q}_{\mathrm{MW}}$, reactor dynamics become invariant of heating pattern as is the case for type 1 configuration at $N_w = 0.06$ ($\overline{q}_{\mathrm{MW}} = 0.0016$), where microwave and conventional heating lead to almost same reactor dynamics at $\Phi_R = 0.1$ as well as at $\Phi_R = 10$ (see the profiles in solid lines). Influence of heating pattern increases with increasing $\overline{q}_{\mathrm{MW}}$ and becomes prominent at sufficiently high intensity of $\overline{q}_{\mathrm{MW}}$, where spatial gradients build up in presence of mass transfer limitations ($\Phi_R \gtrsim 1$) according to the non-uniformity of individual heating pattern. Correspondingly, entire *intermediate* regime of microwave heating with significantly high $\overline{q}_{\mathrm{MW}}$ as well as with volumetric power absorption (except for the region around $N_w \approx 0.25$) leads to much homogenized reactor dynamics compared to conventional heating at $\Phi_R \gtrsim 1$ irrespective of reactor configuration as seen in Figs. (8b) and (9b) for $N_w = 0.5$ and 0.75. Microwave heating also exhibits homogenization in *thin* regime for type 2 configuration, where $\overline{q}_{\mathrm{MW}}$ is not insignificantly small (see profiles of Fig. 6(b) in dashed lines). Highly one sided power absorption near the region around $N_w = 0.25$ obviously decreases the homogenization ability of microwave heating in spite of extremely high $\overline{q}_{\mathrm{MW}}$ for type 1 configuration and microwave heating also leads to significant concentration gradients within the reactor as seen in Fig. 7(b) for $N_w = 0.25$. Similarly, microwave and conventional heating lead to almost similar spatial gradients at $N_p = 3$ as shown in Fig. 10.

Superior homogenization ability of microwave heating over conventional heating becomes irrelevant in the limit of $\Phi_R \ll 1$, where faster diffusion than consumption of reactant homogenizes the concentration gradients irrespective of heating patterns. However, magnitude of Φ_R required to reach this limit depends on the non-uniformity of heating/reaction pattern and hence on $\overline{q}_{\mathrm{MW}}$ for conventional heating. Faster diffusion of reactant at $\Phi_R = 0.1$ is observed to completely homogenize the concentration gradients for all the cases of microwave heating in volumetric power absorption regimes (i.e. for $N_w = 0.06$, 0.5 and 0.75 (Figs. 6(a), 8(a) and 9(a), respectively). Concentration gradients within conventional reactors are also completely homogenized at $\Phi_R = 0.1$ for low to moderately high $\overline{q}_{\mathrm{MW}}$ corresponding to (i) both type 1 and type 2 configurations at $N_w = 0.06$ [Fig. 6(a)], (ii) type 2 configuration at $N_w = 0.25$ and 0.75 (Figs. 7(a) and 9(a), respectively) and (iii) type 1 configuration at $N_w = 0.5$ (Fig. 8(a)). However, concentration gradients within conventional reactors are not completely homogenized at $\Phi_R = 0.1$ for cases of significantly high $\overline{q}_{\mathrm{MW}}$ corresponding to (i) type 1 configuration at $N_w = 0.25$ and 0.75 and (ii) type 2 configuration at $N_w = 0.5$. In such cases, conventional reactors exhibit slight concentration gradients at $\Phi_R = 0.1$, which disappear with further decrease of Thiele modulus. For the same reason, slight concentration gradients are also observed at $\Phi_R = 0.1$ for both microwave and conventional heating at $N_p = 3$ (see Fig. 10(a)).

7. Savings of energy under microwave heating: influence of metallic coating

Since same heating rate is maintained, variations of energy consumption in microwave heating result from the differences in total processing time compared to conventional heating. For an endothermic reaction, changes in processing time are mainly caused by the diffusion time required by the reactant to reach the heating zone/zones from the colder regions of the reactor prior to the occurrence of reaction. It is obvious that volumetric supply of heat reduces diffusion time in microwave heating compared to the highly one sided conventional heating, where reactants from cold right end of the reactor have to diffuse the entire reactor width to avail the heat and react. As a result, microwave heating reduces the processing time as seen in all the $\overline{c}_A$vs τ diagrams of Figs. 6–10 especially for $\Phi_R = 10$. Associated reduction of energy consumption can be quantified as

$$\eta_{\mathrm{MW}} = \left(1 - \frac{\tau_{f_{\mathrm{MW}}}}{\tau_{f_{\mathrm{Conv}}}}\right) \times 100, \tag{13}$$

where η_{MW} determines percentage savings of energy in microwave heating compared to conventional heating. Extent of energy savings obviously depends on the homogenization ability of microwave heating and thus changes with reactor dimension (N_w) as well as reactor configuration as reflected in the $\overline{c}_A$vs τ diagrams of Figs. 6–10. These changes are quantified in Fig. 11(a)–(b), which shows the variations of η_{MW} with N_w (solid lines) over the entire range of *thin* to *thick* regimes at various Thiele modulus of $\Phi_R = 0.1$, 1 and 10 for type 1 [subplot (a)] and type 2 [subplot (b)] configurations. Corresponding $\overline{q}_{\mathrm{MW}}$ vs N_w diagrams are also shown by dotted lines in Fig. 11(a) and (b). As expected, savings of energy under microwave heating increases with increasing mass transfer limitations (Thiele modulus) and becomes prominent for $\Phi_R \geq 1$, where microwave heating can potentially reduce energy consumption as reflected in the magnitude of η_{MW}. Fig. 11 shows the role of reactor dimension (N_w) to maximize the utilization of microwave energy for a given reactor configuration. Fig. 11 also shows the role of metallic coating to further enhance the energy savings at specific reactor dimension. It may be noted that savings of energy can be significantly enhanced at $N_w = 0.5n - 0.25$ by selecting reactors with metallic coating as in type 1 configuration. On the other hand, metallic coating should be avoided at $N_w = 0.5n$ as well as in *thin* regime ($N_w \leq 0.1$). Obviously, savings of energy remain uninfluenced by metallic coating in *thick* regime.

It follows from the discussion on Figs. 6–10 that two factors given by (i) variations of the homogeneity of power absorption pattern and (ii) changes in the magnitude of $\overline{q}_{\mathrm{MW}}$ influence the variations of η_{MW} as N_w varies from *thin* to *thick* regimes. It may be noted from Fig. 5 that changes in the homogeneity of power absorption with N_w are much lower compared to the changes of $\overline{q}_{\mathrm{MW}}$ over the entire volumetric power absorption regime of $N_p < 3$. Correspondingly, η_{MW} mostly follows the variations of $\overline{q}_{\mathrm{MW}}$ for $N_p < 3$ in both Fig. 11(a) and (b) except for a very small region near $N_w = 0.5$ in case of type 1 configuration as shown by shading in Fig. 11(a). It may be noted that as N_w increases within the shaded region of Fig. 11(a), η_{MW} increases while $\overline{q}_{\mathrm{MW}}$ undergoes a reduction. This anomaly interestingly leads to an additional peak in η_{MW} at $N_w = 0.52$ for type 1 configuration in presence of mass transfer limitations as may be observed from Fig. 11(a) for $\Phi_R = 1$ and 10.

Anomalous variations of $\overline{q}_{\mathrm{MW}}$ within the shaded region of Fig. 11(a) are due to the changes in homogeneity of absorbed power,

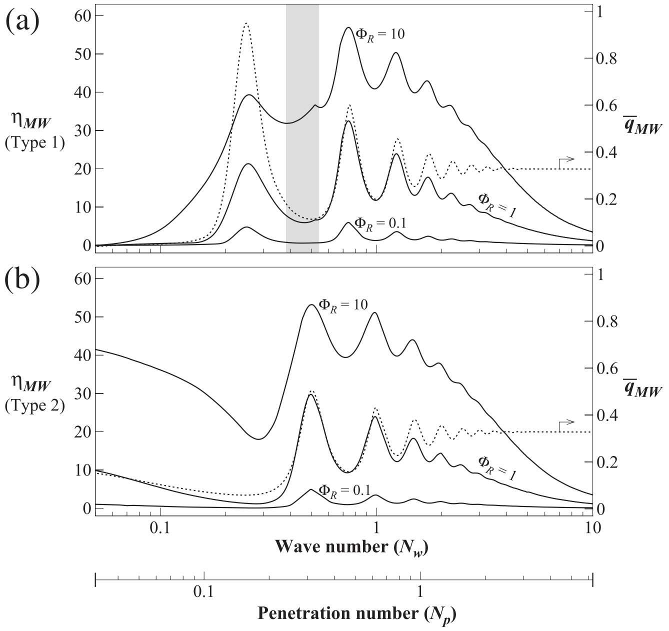

Fig. 11. Variations of η_{MW} with N_w over the range of *thin* to *thick* regimes ($0.05 \leq N_w \leq 10$) for (a) type 1 and (b) type 2 configurations corresponding to $f_w = 0.1$, $f_p = 0.1$, $\tau_D = 1.0$, $N_R = 0.1$, $\beta = 0.1$, $\gamma_R = 10$ and varying Thiele modulus as $\Phi_R = 0.1$, 1 and 10. Corresponding $\overline{q}_{\mathrm{MW}}$ vs N_w diagrams are also shown in dotted lines (corresponding scale is shown at right axis).

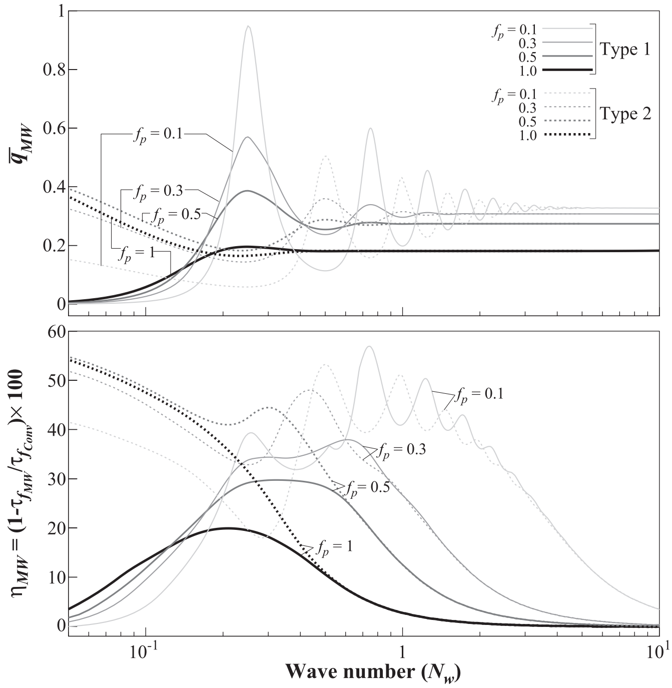

Fig. 12. Influence of f_p on variation patterns of $\bar{q}_{\mathrm{MW}}$ and η_{MW} with N_w for type 1 (solid lines) and type 2 (dotted lines) configurations at $f_w = 0.1$ and $\Phi_R = 10$.

which undergoes a significant transformation from $N_w = 0.1$ to 0.5 irrespective of the reactor configuration as shown in the insets of Fig. 5. It may be noted that homogeneity of power absorption reduces drastically from $N_w = 0.1$ to $N_w = 0.25$ and then reverts back as N_w increases to 0.5. Increasing homogeneity of absorbed power causes η_{MW} to increase from $N_w \approx 0.4$ to $N_w \approx 0.5$ (more specifically from $N_w = 0.38$ to 0.52 at $\Phi_R = 10$ and from $N_w = 0.45$ to 0.52 at $\Phi_R = 1$) in spite of decreasing $\bar{q}_{\mathrm{MW}}$ for type 1 configuration. It may be noted that reduction of $\bar{q}_{\mathrm{MW}}$ are not significant within the shaded region. On the other hand, changes of $\bar{q}_{\mathrm{MW}}$ are exceptionally high within the range of $0.15 \lesssim N_w \lesssim 0.4$ for type 1 configuration and hence η_{MW} follows the same regardless of the changes of homogeneity of power absorption. This causes η_{MW} to increase from $N_w = 0.1$ to 0.25 for type 1 configuration in spite of decreasing homogeneity of absorbed power. Similarly, η_{MW} decreases from $N_w = 0.25$ to $N_w \approx 0.4$ in Fig. 11(a) although homogeneity of power absorption increases over that range. However, changes in the homogeneity of power absorption suppress the variations of η_{MW} at $N_w = 0.25$ compared to the corresponding resonating peak of $\bar{q}_{\mathrm{MW}}$ as may be observed from Fig. 11(a). Also, since mass transfer limitations bring out the effect of varying homogeneity of absorbed power distribution, the region of anomalous variations of η_{MW} also shrinks with decreasing Φ_R and disappear at $\Phi_R = 0.1$. In contrast to type 1 configuration, influence of the variations of $\bar{q}_{\mathrm{MW}}$ corroborate with influence of changing homogeneity of power absorption over the entire range of $0.1 \le N_w \le 0.5$ for type 2 configuration and η_{MW} shows one-to-one correspondence with $\bar{q}_{\mathrm{MW}}$ in Fig. 11(b) for the entire range of $N_p < 3$ irrespective of Thiele modulus.

8. Effect of f_p on influence of metallic coating

Influence of f_p on $\bar{q}_{\mathrm{MW}}$ over the entire range of *thin* to *thick* regimes ($0.05 \le N_w \le 10$) and associated changes in η_{MW} at $\Phi_R = 10$ for type 1 and type 2 configurations are shown in Fig. 12 by increasing f_p from 0.1 to its upper bound of 1 [Note that f_p is bound within 0–1 according to Eq. (A.3)]. In Fig. 12, solid and dotted lines represent type 1 and type 2 configurations, respectively. Here, mass transfer limited situations of $\Phi_R = 10$ is selected to prominently bring out the effect of f_p on η_{MW}. All the simulations in Fig. 12 are performed at $f_w = 0.1$ with all other parameters to be same as in previous figures. Fig. 12 shows that resonances of power absorption are strongly affected by f_p, where resonating peaks of $\bar{q}_{\mathrm{MW}}$ gradually disappear as f_p increases beyond 0.5 (or $1.5/\pi$ more precisely [62]). It may be noted that most of the resonating peaks of $\bar{q}_{\mathrm{MW}}$, except the first few, disappear even at $f_p = 0.3$ for both the configurations. With suppression of resonances, *intermediate* regime also shrinks and causes its volumetric power absorption to transform to the highly one sided distribution of *thick* regime as f_p increases from 0.1 to $>1.5/\pi$ as illustrated in Fig. 13. Fig. 13 shows the transformation of power absorption profiles in type 1 and type 2 configurations as f_p increases from 0.1 (solid line) to 0.5 (dashed line) and 1 (dotted line) at $N_w = 0.06$, 0.25, 0.5 and 0.75 for $f_w = 0.1$. As power absorption transforms towards the highly one sided distribution of *thick* regime, influence of metallic coating also gradually decreases with increasing f_p as shown in Fig. 13. It may be noted that power absorption profiles of $N_w = 0.5$ and 0.75 become invariant of the reactor configuration beyond $f_p = 0.5$. Correspondingly, region of influence of reactor configuration on $\bar{q}_{\mathrm{MW}}$ shrinks considerably from $N_w \le 5$ at $f_p = 0.1$ to $N_w \le 1.5$, 0.9 and 0.5 at $f_p = 0.3$, 0.5 and 1, respectively (see Fig. 12). As a result, η_{MW} also shows a decreasing region of influence of reactor configuration from $N_w \le 4$ to $N_w \le 1.5$, 0.6 and 0.5 as f_p increases from $f_p = 0.1$ to $f_p = 0.3$, 0.5 and 1 respectively.

Transformation to highly one sided power absorption profiles reduces the homogeneity of microwave heating as f_p increases from 0.1 to 1 for $N_w \ge 0.5$, Correspondingly, Fig. 12 shows a significant reduction of η_{MW} from $f_p = 0.1$ to 1 for both type 1 and type 2 configurations over the entire range of $N_w \ge 0.5$. Over this range of

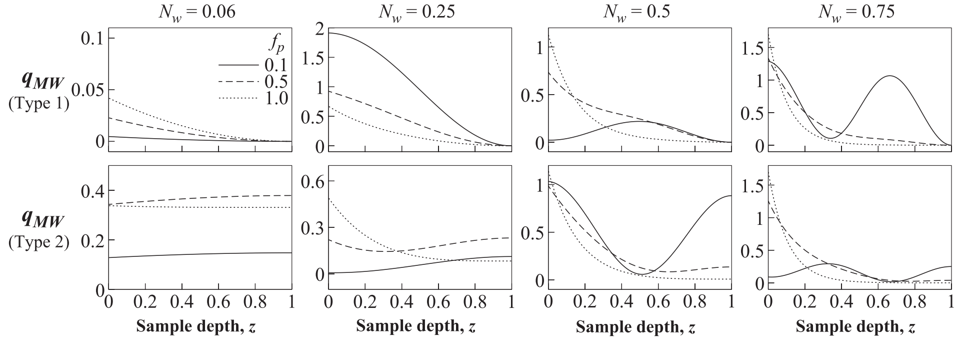

Fig. 13. Variations of power absorption profiles of type 1 and type 2 configurations from $f_p = 0.1$ (solid lines) to 0.5 (dashed lines) and 1 (dotted lines) at $f_w = 0.1$ and $N_w = 0.06$, 0.25, 0.5 and 0.75.

$N_w \geq 0.5$, influence of reducing homogeneity of microwave heating on $\eta_{\rm MW}$ either dominates or follows the influence of varying $\overline{q}_{\rm MW}$ from $f_p = 0.1$ to 1. In contrast, homogeneity of microwave heating does not alter significantly with f_p in *thin* regime (as shown in Fig. 13 for $N_w = 0.06$) and $\eta_{\rm MW}$ follows the variations of $\overline{q}_{\rm MW}$ for $N_w \leq 0.1$ as seen in Fig. 12. In between $0.1 \leq N_w \leq 0.5$, changes in both homogeneity of power absorption and intensity of $\overline{q}_{\rm MW}$ combinedly influence $\eta_{\rm MW}$ as reflected in its complex variation patterns from $f_p = 0.1$ to 1 within that range (see Fig. 12).

9. Effect of f_w on influence of metallic coating

Parameter $f_w = \lambda_{\rm eff}/\lambda_0$ alters relative magnitude of microwave wavelength within the sample compared to that in free space, which in turn alters scattering of microwaves from reactor walls via Eqs. (5d) and (5e). Associated changes in power absorption patterns for type 1 and type 2 configurations are shown in Fig. 14 for representative reactor dimensions of $N_w = 0.06$, 0.25, 0.5 and 0.75, while the corresponding changes in $\overline{q}_{\rm MW}$ are shown in Fig. 15 over the entire range of $0.05 \leq N_w \leq 10$. In both the figures (Figs. 14 and 15), f_w is varied from 0.1 (solid line) to 0.5 (dashed line) and 1 (dotted line) while f_p is kept constant at 0.1. It may be noted that similar to f_p, f_w is also bound between 0 and 1 ($0 \leq f_w \leq 1$) as wavelength of microwave is maximum in vacuum or free space. Fig. 15 also illustrates the corresponding changes of $\eta_{\rm MW}$ at $\Phi_R = 10$ (similar to Fig. 12), where other parameters used in the simulations are same as in previous figures (i.e. $\tau_D = 1$, $N_R = 0.1$, $\beta = 0.1$ and $\gamma_R = 10$).

It may be noted from Fig. 14 that unlike f_p, influence of f_w on power absorption pattern does not follow a specific trend and depends strongly on reactor dimension as well as reactor configuration. Power absorption pattern remains almost unchanged from $f_w = 0.1$ to 1 in case of type 1 configuration, while f_w significantly alters power absorption patterns for type 2 configuration for all the cases except for $N_w = 0.06$ corresponding to *thin* regime (see Fig. 14). On the other hand, both the configurations interestingly show similar variations of $\overline{q}_{\rm MW}$ with suppression of resonating peaks from $f_w = 0.1$ to 1 as well as higher magnitudes of $\overline{q}_{\rm MW}$ at $f_w = 0.5$ and 1 compared to those at $f_w = 0.1$ over the entire *intermediate* regime except near the boundary of *thin* regime ($0.1 < N_w < 0.5$) (see Fig. 15). Accordingly, $\eta_{\rm MW}$ also shows higher magnitudes at $f_w = 0.5$ and 1 compared to those at $f_w = 0.1$ over most of the *intermediate* regime along with suppression of oscillations as f_w increases from 0.1 to 1 in Fig. 15 for both type 1 and type 2 configurations. These transformations of $\eta_{\rm MW}$ interestingly alter the range of reactor dimension for selection of either type 1 or type 2 configuration in order to enhance $\eta_{\rm MW}$. At $f_w = 0.5$ and 1, type 1 configuration can effectively enhance $\overline{q}_{\rm MW}$ or $\eta_{\rm MW}$ over most of the *intermediate* regime. This is in contrast to the case of $f_w = 0.1$, where type 1 configuration preferentially enhances $\overline{q}_{\rm MW}$ and hence $\eta_{\rm MW}$ only around the resonating peaks at $N_w = 0.5 - 0.25n$ as may be observed from Fig. 15. The region of preferential enhancement of $\eta_{\rm MW}$ by type 1 configuration expands to $N_w \geq 0.6$ and $N_w \geq 0.45$ at $f_w = 0.5$ and 1, respectively. On the other hand, type 1 configuration no longer remains effective to enhance $\eta_{\rm MW}$ near $N_w = 0.25$ at $f_w = 0.5$ and 1 as may be observed from Fig. 15. Instead, type 2 configuration becomes efficient choice to enhance $\eta_{\rm MW}$ till $N_w \leq 0.6$ and $N_w \leq 0.45$ at $f_w = 0.5$ and 1 respectively in spite of lower $\overline{q}_{\rm MW}$ than type 1 configuration around $N_w = 0.25$. This is due to the transformation of power absorption pattern with f_w as illustrated in Fig. 14, which shows that highly one sided power absorption of $N_w = 0.25$ at $f_w = 0.1$ transforms to volumetric power absorption at $f_w = 0.5$ and 1 for type 2 configuration. On the other hand, power absorption for type 1 configuration remains to be one sided for all the f_w's. Correspondingly, influence of homogenized heating under type 2 configuration at $f_w = 0.5$ and 1 dominate and $\eta_{\rm MW}$ remains to be higher in type 2 configuration around $N_w = 0.25$ for $f_w = 0.5$ and 1 as observed in Fig. 15.

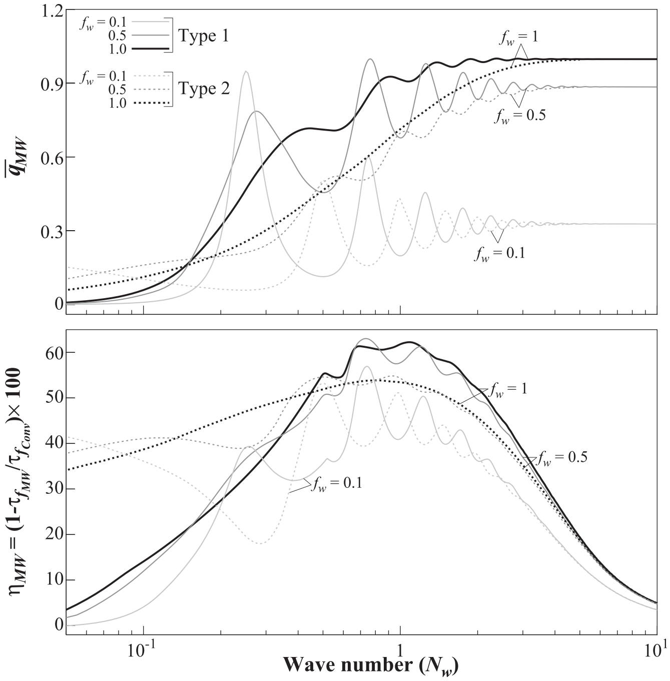

Fig. 15. Influence of f_w on variation patterns of $\overline{q}_{\rm MW}$ and $\eta_{\rm MW}$ with N_w for type 1 (solid lines) and type 2 (dotted lines) configurations at $f_p = 0.1$ and $\Phi_R = 10$.

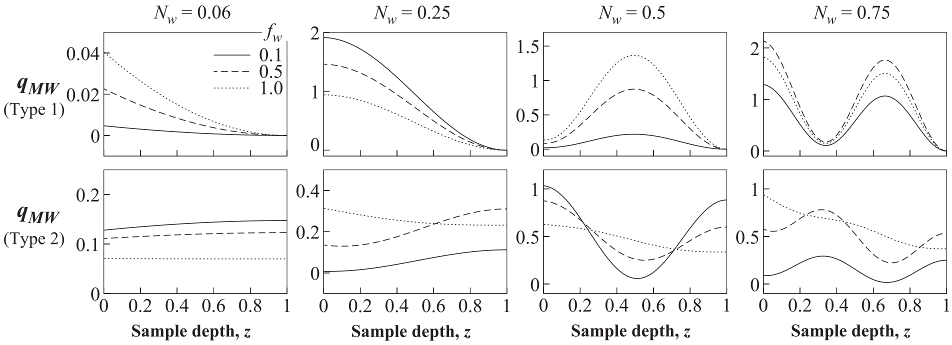

Fig. 14. Variations of power absorption profiles of type 1 and type 2 configurations from $f_w = 0.1$ (solid lines) to 0.5 (dashed lines) and 1 (dotted lines) at $f_p = 0.1$ and $N_w = 0.06$, 0.25, 0.5 and 0.75.

10. Summary and conclusive remarks

This work presents a theoretical basis for probable energy savings under microwave heating for conducting an endothermic gas phase reaction and shows the role of metallic coating in enhancing the savings of energy in places where savings are not significant otherwise. The reaction is assumed to occur in presence of susceptors within a semiinfinite batch reactor and total power consumption under microwave heating are compared with those under equivalent conventional heating. The analysis presented in this work are based on single mode microwave radiations, which can be easily achieved within any custom made waveguide. The entire assembly of reactor with packed susceptors can be placed in the test section of the waveguide, which can be further customized by applying a metal coated film on the opposite side of wave propagation to investigate the reactor dynamics with and without the metal coated film. It may be noted that single mode microwaves not only reduce complexity of the mathematical model without destroying the essential physics but also cause much higher power absorption than multi mode microwaves. The analysis has been performed by simulating reactor progress from detailed mass and energy balance equations in conjunction with Helmholtz equation of wave propagation by using weak formulation of Galerkin finite element method and Crank-Nicholson time integration scheme. In all the simulations, same heating rates are maintained in microwave and conventional heatings to make them comparable and equivalent to each other.

This work considers probable *uniform*, *oscillatory* and *exponentially attenuated* microwave heating patterns of *thin* ($N_w \le 0.1$), *intermediate* [$0.1 < N_w < 3/(2\pi f_p)$] and *thick* ($2\pi N_w f_p$ or $N_p \ge 3$) regimes and simulates them by varying reactor dimension ($2L/\lambda_{\text{eff}}$) over the range $0.05 \le N_w \le 10$ for both the cases of with and without metallic coating. The analysis shows that microwave heating homogenizes reactor dynamics and can save as much as 60% energy consumption based on regime of operation (reactor dimension, dielectric properties of the susceptors and transport limitations within the reactor). This analysis shows efficient use of metallic coating in enhancing savings of energy consumption under microwave heating for reactor dimensions around $N_w = 0.5n - 0.25$, $n = 1,2\ldots$, where otherwise microwave heating leads to very slow reaction and less energy savings. For example, savings of energy doubles from 20% to 40% in presence of metallic coating at $N_w = 0.25$ for significant mass transfer limitations within the reactor corresponding to $\Phi_R = 10$. Similarly, metallic coating enhances saving of energy from 40% to 60% and 50% at $N_w = 0.75$ and 1.25, respectively. On the other hand, metallic coatings are shown to be avoided at resonating reactor dimensions without metallic coating corresponding to $N_w = 0.5n$, $n = 1,2\ldots$ as well as for reactors in *thin* regime.

This work quantifies probable savings of energy under microwave heating (η_{MW}) as reactor dimension varies from *thin* to *thick* regimes and identifies the ranges of reactors where metallic coating can efficiently reduce energy consumption. These results can be used as basis for appropriate selection of reactor configuration (with or without metallic coating) for a given reactor dimension as well as to select reactor dimension in order to maximize utilization of microwave energy. This work also quantifies changes in energy savings due to changing dielectric properties of the reacting medium and shows how tuning of susceptor material in conjunction with appropriate selection of reactor configuration (with or without metallic coating) can play an important role in enhancing energy utilization via microwave heating.

Reduction of energy consumption is one of the important factors in determining sustainability of microwave heating compared to conventional heating to conduct chemical reaction. In that context, it becomes extremely essential to analyze relative energy consumption under microwave heating compared to that required for conventional heating to achieve desired yield. However, majority of the previous work only concentrated on the chemistry aspect of the process and reported the extent of enhancement of reaction for a variety of reacting systems under different reaction conditions. Till date, only a very few studies exist, which report comparative measurement of energy consumption under microwave heating and equivalent conventional heating [42–44,48,55,57]. The observations of these works are summarized in Table 1. It is interesting to note that current simulations also predict similar range of energy savings as measured/estimated in earlier work (especially those reported in the last five entries of Table 1 [42–44,48,55]) even though the reacting systems differ completely from the present setup. It is important to note that Table 1 summarizes only those results corresponding to similar operating parameters for microwave and conventional heating (e.g. reaction volume, reaction temp etc.). As noted in the previous works [42–44,48,55,57], savings of energy can vary widely depending on operating parameters and even with the specific microwave unit used for the reactions. Also, reaction volume, reacting medium, mode of operation (continuous or batch) can significantly affect the energy savings among many other factors. Thus, it has been recommended by previous researchers to do a case-to-case basis energy consumption analysis to study the viability of the process. In that context, the present simulations may act as basic guidelines to design appropriate reactor setup with or without metallic coating in order to maximize energy utilization.

Table 1
Literature data regarding relative savings of energy under microwave heating compared to conventional heating at similar operating conditions (reactor size, reaction temperature etc.

Reference	Reaction	Energy savings	Comment
[57]	Heterogenous Suzuki	98%	Preliminary calculations
	Friedel–Crafts acetylation	90%	
[55]	Biodiesel production	4%–73%	(Depending on operating condition)
[48]	S_NAr reaction at 140 °C	66%	MARS MW unit
	Alkylation reaction at 150 °C	59%	
	Heck reaction at 140 °C	54%	
[44]	Diels–Alder reaction	11% & 71%	MARS unit at 140 °C for 120 min & at 180 °C for 8 min, respectively
[43]	FFA removal by esterification	37%	
[42]	Hantzsch dihydropyridine synthesis	65%	Multimode MW unit

Acknowledgment

Authors would like to thank anonymous reviewers for critical comments and suggestions which improved the quality of the manuscript.

Appendix A. Electromagnetic equations for evaluation of Q_{MW}

Propagation of microwave within a semiinfinite domain with dielectric packings shown in Fig. 1 can be characterized by the following Helmholtz equation [65] for both type 1 and type 2 configurations:

$$\frac{d^2E_m}{dZ^2} + \left(\frac{2\pi}{\lambda_{\text{eff}}} + i\frac{1}{D_{p_{\text{eff}}}}\right)^2 E_m = 0 \tag{A.1}$$

and associated power absorption can be expressed as

$$Q_{\mathrm{MW}}(Z) = \frac{c\varepsilon_0\lambda_0}{\lambda_{\mathrm{eff}}D_{p_{\mathrm{eff}}}}E_m(Z)E_m(Z)^*. \tag{A.2}$$

In the above equations, E_m is microwave induced electric field, c is velocity of light, ε_0 is free space permittivity, $\lambda_0 = c/f$ is wavelength of microwave in free space and λ_{eff} and $D_{p_{\mathrm{eff}}}$ are effective wavelength and penetration depth of microwave within the packed domain of Fig. 1, respectively given by

$$\lambda_{\mathrm{eff}} = \frac{2c}{f}\left[2\left(\sqrt{\kappa'^2_{\mathrm{eff}} + \kappa''^2_{\mathrm{eff}}} + \kappa'_{\mathrm{eff}}\right)\right]^{-1/2} \tag{A.3a}$$

$$D_{p_{\mathrm{eff}}} = \frac{c}{\pi f}\left[2\left(\sqrt{\sqrt{\kappa'^2_{\mathrm{eff}} + \kappa''^2_{\mathrm{eff}}} - \kappa'_{\mathrm{eff}}}\right)\right]^{-1/2}, \tag{A.3b}$$

where κ'_{eff} and κ''_{eff} are effective dielectric constant and effective dielectric loss of the packed domain, respectively and f is frequency of incident radiation. Electromagnetic wave undergoes scattering at the interface of free space and power absorbing medium in absence of metallic surface/coating, which can be mathematically represented by radiation boundary condition for E_m [76]. Radiation boundary condition at the left wall is given

$$@Z = -L : \frac{\mathrm{d}E_m}{\mathrm{d}Z} + i\frac{2\pi}{\lambda_0}E_m = i\frac{4\pi}{\lambda_0}E_0 \exp\left[-i\frac{2\pi}{\lambda_0}L\right], \tag{A.4}$$

for both type 1 and type 2 configurations, where $E_0 = \sqrt{2I_0/c\varepsilon_0}$ is the incident electric field. Radiation boundary condition for the right wall of type 2 reactor with no metallic coating is given by

$$@Z = L : \frac{\mathrm{d}E_m}{\mathrm{d}Z} - i\frac{2\pi}{\lambda_0}E_m = 0 \text{ for type 2.} \tag{A.5a}$$

On the other hand, metallic coating completely reflects electromagnetic wave in type 1 reactor and associated boundary condition can be written as

$$@Z = L : E_m = 0 \text{ for type 1.} \tag{A.5b}$$

The description of electromagnetic wave propagation through packed dielectrics under consideration is complete with appropriate correlations κ'_{eff} and κ''_{eff}. Most widely accepted correlations were first developed by Fricke [77], which considers the effect of porosity (ϕ) and dispersity of packings in addition to the dielectric properties of packing material (κ'_p and κ''_p)

$$\kappa'_{\mathrm{eff}} + i\kappa''_{\mathrm{eff}} = \frac{\left(\kappa'_p + i\kappa''_p\right)\left[1 + a\phi + a\left(\kappa'_p + i\kappa''_p\right)(1-\phi)\right]}{1 - \phi + \left(\kappa'_p + i\kappa''_p\right)(a + \phi)}, \tag{A.6}$$

where $a = 2$ for spherical and 1 for cylindrical packings.

Appendix B. Analytical expressions for absorbed power and their inner products

Solving Helmholtz equation (Eq. (5c)) and associated radiation boundary conditions (Eqs. (5d) and (5e)), analytical expressions for absorbed power (q_{MW}) can be written as

$$q_{\mathrm{MW}} = \frac{16\pi N_w f_p f_w\left[\cosh 2N_p(1-z) - \cos 4\pi N_w(1-z)\right]}{c_1\cos 4\pi N_w + c_2\cosh 2N_p + c_3\sin 4\pi N_w + c_4\sinh 2N_p} \tag{B.1}$$

for type 1 reactor with metallic coating and

$$q_{\mathrm{MW}} = \frac{16\pi N_w f_p f_w\begin{bmatrix} c_2\cosh 2N_p(1-z) + c_4\sinh 2N_p(1-z) \\ +c_1\cos 4\pi N_w(1-z) + c_3\sin 4\pi N_w(1-z)\end{bmatrix}}{(c_3^2 - c_1^2)\cos 4\pi N_w + (c_2^2 + c_4^2)\cosh 2N_p - 2c_1c_3\sin 4\pi N_w + 2c_2c_4\sinh 2N_p} \tag{B.2}$$

for type 2 reactor configuration without metallic coating, where coefficients c_1–c_4 are given by

$$c_1 = 1 + f_p^2 - f_w^2, \tag{B.3a}$$

$$c_2 = 1 + f_p^2 + f_w^2, \tag{B.3b}$$

$$c_3 = -2f_p f_w, \tag{B.3c}$$

$$c_4 = 2f_w. \tag{B.3d}$$

Using the above expressions for absorbed power, the expression of $\langle q_{\mathrm{MW}}, w_n\rangle$ for $n \neq 0$ can be written as

$$\langle q_{\mathrm{MW}}, w_n\rangle = \frac{4\sqrt{2}f_w\left[\dfrac{\sinh 2N_p}{1 + \dfrac{n^2\pi^2}{4N_p^2}} - \begin{cases} 2\pi N_w f_p \cos 4\pi N_w & n = 4N_w \\ \dfrac{f_p \sin 4\pi N_w}{1 - \dfrac{n^2\pi^2}{16\pi^2 N_w^2}} & n \neq 4N_w \end{cases}\right]}{c_1\cos 4\pi N_w + c_2\cosh 2N_p + c_3\sin 4\pi N_w + c_4\sinh 2N_p}, \tag{B.4a}$$

for type 1 reactor with metallic coating and

$$\langle q_{\mathrm{MW}}, w_n \rangle = \frac{4\sqrt{2}f_w \left[\dfrac{c_2 \sinh 2N_p + c_4\left(\cosh 2N_p - (-1)^n\right)}{1 + \dfrac{n^2\pi^2}{4N_p^2}} + \begin{cases} 2\pi N_w f_p\left(c_1 \cos 4\pi N_w + c_3 \sin 4\pi N_w\right) & n = 4N_w \\ \dfrac{f_p\left(c_1 \sin 4\pi N_w + c_3\left[(-1)^n - \cos 4\pi N_w\right]\right)}{1 - \dfrac{n^2\pi^2}{16\pi^2 N_w^2}} & n \neq 4N_w \end{cases} \right]}{\left(c_3^2 - c_1^2\right)\cos 4\pi N_w + \left(c_2^2 + c_4^2\right)\cosh 2N_p - 2c_1c_3 \sin 4\pi N_w + 2c_2c_4 \sinh 2N_p} \tag{B.4b}$$

for type 2 reactor configuration without metallic coating. Similarly, the expressions for $\langle q_{\mathrm{MW}}, w_0 \rangle \equiv \langle q_{\mathrm{MW}}, 1 \rangle = \bar{q}_{\mathrm{MW}}$ can be written as

$$\bar{q}_{\mathrm{MW}} = \frac{4f_w\left[\sinh 2N_p - f_p \sin 4\pi N_w\right]}{c_1 \cos 4\pi N_w + c_2 \cosh 2N_p + c_3 \sin 4\pi N_w + c_4 \sinh 2N_p} \tag{B.5a}$$

and

$$\bar{q}_{\mathrm{MW}} = \frac{4f_w\left[c_2 \sinh 2N_p + c_4\left(\cosh 2N_p - 1\right) + f_p\left(c_1 \sin 4\pi N_w + c_3\left(1 - \cos 4\pi N_w\right)\right)\right]}{\left(c_3^2 - c_1^2\right)\cos 4\pi N_w + \left(c_2^2 + c_4^2\right)\cosh 2N_p - 2c_1c_3 \sin 4\pi N_w + 2c_2c_4 \sinh 2N_p} \tag{B.5b}$$

for type 1 and type 2 reactor configurations, respectively.

References

[1] Deora NS, Misra NN, Deswal A, Mishra HN, Cullen PJ, Tiwari BK. Ultrasound for improved crystallisation in food processing. Food Engineering Reviews 2013;5(1):36–44.

[2] Rooze J, Rebrov EV, Schouten JC, Keurentjes JTF. Dissolved gas and ultrasonic cavitation – a review. Ultrasonics Sonochemistry 2013;20(1):1–11.

[3] Eren Z. Ultrasound as a basic and auxiliary process for dye remediation: a review. Journal of Environmental Management 2012;104:127–41.

[4] Veljkovic VB, Avramovic JM, Stamenkovic OS. Biodiesel production by ultrasound-assisted transesterification: state of the art and the perspectives. Renewable and Sustainable Energy Reviews 2012;16(2):1193–209.

[5] Awad TS, Moharram HA, Shaltout OE, Asker D, Youssef MM. Applications of ultrasound in analysis, processing and quality control of food: a review. Food Research International 2012;48(2):410–27.

[6] Shirsath SR, Sonawane SH, Gogate PR. Intensification of extraction of natural products using ultrasonic irradiations – A review of current status. Chemical Engineering and Processing 2012;53:10–23.

[7] Zhang WJ, Yao Y, He BX, Wang RS. The energy-saving characteristic of silica gel regeneration with high-intensity ultrasound. Applied Energy 2011;88(6):2146–56.

[8] Bang JH, Suslick KS. Applications of ultrasound to the synthesis of nanostructured materials. Advanced Materials 2010;22(10):1039–59.

[9] Leonelli C, Mason TJ. Microwave and ultrasonic processing: now a realistic option for industry. Chemical Engineering and Processing 2010;49(9):885–900.

[10] Yao Y. Using power ultrasound for the regeneration of dehumidizers in desiccant air-conditioning systems: a review of prospective studies and unexplored issues. Renewable and Sustainable Energy Reviews 2010;14(7):1860–73.

[11] Cella R, Stefani HA. Ultrasound in heterocycles chemistry. Tetrahedron 2009;65(13):2619–41.

[12] Yao Y, Zhang W, Li S. Feasibility study on power ultrasound for regeneration of silica gel-A potential desiccant used in air-conditioning system. Applied Energy 2009;86(11):2394–400.

[13] Rokhina EV, Lens P, Virkutyte J. Low-frequency ultrasound in biotechnology: state of the art. Trends in Biotechnology 2009;27(5):298–306.

[14] Leveque JM, Cravotto G. Microwaves, power ultrasound, and ionic liquids. A new synergy in green organic synthesis. Chimia 2006;60(6):313–20.

[15] Lifka J, Ondruschka B, Hofmann J. The use of ultrasound for the degradation of organic compounds in water: aquasonolysis – a review. Chemie Ingenieur Technik 2002;74(4):403–13.

[16] Ince NH, Tezcanli G, Belen RK, Apikyan IG. Ultrasound as a catalyzer of aqueous reaction systems: the state of the art and environmental applications. Applied Catalysis B Environmental 2001;29(3):167–76.

[17] Citeau M, Olivier J, Mahmoud A, Vaxelaire J, Larue O, Vorobiev E. Pressurised electro-osmotic dewatering of activated and anaerobically digested sludges: electrical variables analysis. Water Research 2012;46(14):4405–16.

[18] Qi RH, Tian CQ, Shao SQ, Tang MS, Lu L. Experimental investigation on performance improvement of electro-osmotic regeneration for solid desiccant. Applied Energy 2011;88(8):2816–23.

[19] Chien SC, Ou CY. A novel technique of harmonic waves applied electro-osmotic chemical treatment for soil improvement. Applied Clay Science 2011;52(3):235–44.

[20] Ho MY, Chen GH. Enhanced electro-osmotic dewatering of fine particle suspension using a rotating anode. Industrial and Engineering Chemistry Research 2001;40(8):1859–63.

[21] Locke BR, Thagard SM. Analysis and review of chemical reactions and transport processes in pulsed electrical discharge plasma formed directly in liquid water. Plasma Chemistry and Plasma Processing 2012;32(5):875–917.

[22] Yamamoto T, Tanioka G, Okubo M, Kuroki T. Water vapor desorption and adsorbent regeneration for air conditioning unit using pulsed corona plasma. Journal of Electrostatics 2007;65(4):221–7.

[23] Nair SA, Yan K, Pemen AJM, Winands GJJ, van Gompel FM, van Leuken HEM, et al. A high-temperature pulsed corona plasma system for fuel gas cleaning. Journal of Electrostatics 2004;61(2):117–27.

[24] Kim HH. Nonthermal plasma processing for air-pollution control: a historical review, current issues, and future prospects. Plasma Processes and Polymers 2004;1(2):91–110.

[25] Ravasio S, Cavallotti C. Analysis of reactivity and energy efficiency of methane conversion through non thermal plasmas. Chemical Engineering Science 2012;84:580–90.

[26] Malik MA, Malik SA. Pulsed corona discharges and their applications in toxic VOCs abatement. Chinese Journal of Chemical Engineering 1999;7(4):351–62.

[27] Chandrasekaran S, Ramanathan S, Basak T. Microwave material processing-A review. AIChE Journal 2012;58(2):330–63.

[28] Zhang X, Liu Z. Recent advances in microwave initiated synthesis of nanocarbon materials. Nanoscale 2012;4(3):707–14.

[29] Damour C, Hamdi M, Josset C, Auvity B, Boillereaux L. Energy analysis and optimization of a food defrosting system. Energy 2012;37(1):562–70.

[30] Motevali A, Minaei S, Khoshtaghaza MH, Amirnejat H. Comparison of energy consumption and specific energy requirements of different methods for drying mushroom slices. Energy 2011;36(11):6433–41.

[31] Motevali A, Minaei S, Khoshtagaza MH. Evaluation of energy consumption in different drying methods. Energy Conversion and Management 2011;52(2): 1192–9.

[32] Kharissova OV, Kharisov BI, Valdes JJR. Review: the use of microwave irradiation in the processing of glasses and their composites. Industrial and Engineering Chemistry Research 2010;49(4):1457–66.

[33] Mutyala S, Fairbridge C, Pare JRJ, Belanger JMR, Ng S, Hawkins R. Microwave applications to oil sands and petroleum: a review. Fuel Processing Technology 2010;91(2):127–35.

[34] Sharma GP, Prasad S. Specific energy consumption in microwave drying of garlic cloves. Energy 2006;31(12):1921–6.

[35] Zhang M, Tang J, Mujumdar AS, Wang S. Trends in microwave-related drying of fruits and vegetables. Trends in Food Science and Technology 2006;17(10): 524–34.

[36] Kingman SW. Recent developments in microwave processing of minerals. International Material Review 2006;51(1):1–12.

[37] Jones DA, Lelyveld TP, Mavrofidis SD, Kingman SW, Miles NJ. Microwave heating applications in environmental engineering – a review. Resources Conservation and Recycling 2002;34(2):75–90.

[38] Sumnu G. A review on microwave baking of foods. International Journal of Food Science and Technology 2001;36(2):117–27.

[39] Haque KE. Microwave energy for mineral treatment processes - a brief review. International Journal of Mineral Processing 1999;57(1):1–24.

[40] Chen KS, Lin YC, Hsu KH, Wang HK. Improving biodiesel yields from waste cooking oil by using sodium methoxide and a microwave heating system. Energy 2012;38(1):151–6.

[41] Wang MJ, Huang YF, Chiueh PT, Kuan WH, Lo SL. Microwave-induced torrefaction of rice husk and sugarcane residues. Energy 2012;37(1):177–84.

[42] Devine WG, Leadbeater NE. Probing the energy efficiency of microwave heating and continuous-flow conventional heating as tools for organic chemistry. Arkivoc 2011;Part 5:127–43.

[43] Kim D, Choi J, Kim GJ, Seol SK, Ha YC, Vijayan M, et al. Microwave-accelerated energy-efficient esterification of free fatty acid with a heterogeneous catalyst. Bioresource Technology 2011;102(3):3639–41.

[44] Godwin DR, Lawton SJ, Moseley JD, Welham MJ, Weston NP. Energy efficiency of conventionally-heated pilot plant reactors compared with microwave reactors. Energy and Fuels 2010;24:5446–53.

[45] Lam SS, Russell AD, Chase HA. Microwave pyrolysis, a novel process for recycling waste automotive engine oil. Energy 2010;35(7):2985–91.

[46] Strauss CR, Rooney DW. Accounting for clean, fast and high yielding reactions under microwave conditions. Green Chemistry 2010;12(8):1340–4.

[47] Durka T, Van Gerven T, Stankiewicz A. Microwaves in heterogeneous gas-phase catalysis: experimental and numerical approaches. Chemical Engineering and Technology 2009;32(9):1301–12.

[48] Moseley JD, Woodman EK. Energy efficiency of microwave- and conventionally heated reactors compared at meso scale for organic reactions. Energy and Fuels 2009;23:5438–47.

[49] Polshettiwar V, Nadagouda MN, Varma RS. Microwave-assisted chemistry: a rapid and sustainable route to synthesis of organics and nanomaterials. Australian Journal of Chemistry 2009;62(1):16–26.

[50] Cherbanski R, Molga E. Intensification of desorption processes by use of microwaves – an overview of possible applications and industrial perspectives. Chemical Engineering and Processing 2009;48(1):48–58.

[51] Kappe CO. Microwave dielectric heating in synthetic organic chemistry. Chemical Society Reviews 2008;37(6):1127–39.

[52] Bowman MD, Holcomb JL, Kormos CM, Leadbeater NE, Williams VA. Approaches for scale-up of microwave-promoted reactions. Organic Process Research and Development 2008;12(1):41–57.

[53] Wei ZS, Du ZY, Lin ZH, He HM, Qiu RL. Removal of NO(x) by microwave reactor with ammonium bicarbonate and Ga-A zeolites at low temperature. Energy 2007;32(8):1455–9.

[54] Cecilia R, Kunz U, Turek T. Possibilities of process intensification using microwaves applied to catalytic microreactors. Chemical Engineering and Processing 2007;46(9):870–81.

[55] Barnard TM, Leadbeater NE, Boucher MB, Stencel LM, Wilhite BA. Continuous-flow preparation of biodiesel using microwave heating. Energy and Fuels 2007;21(3):1777–81.

[56] Tokuyama H, Nakamura M. Acceleration of reaction by microwave irradiation. Journal of Synthetic Organ Chemistry Japan 2005;63(5):523–38.

[57] Gronnow MJ, White RJ, Clark JH, Macquarrie DJ. Energy efficiency in chemical reactions: a comparative study of different reaction techniques. Organic Process Research and Development 2005;9(4):516–8.

[58] Nuchter M, Ondruschka B, Bonrath W, Bonrath W, Gum A. Microwave assisted synthesis – a critical technology overview. Green Chemistry 2004;6(3):128–41.

[59] Nuchter M, Muller U, Ondruschka B, Tied A, Lautenschlager W. Microwave-assisted chemical reactions. Chemical Engineering and Technology 2003;26(12):1207–16.

[60] Akyel C, Bilgen E. Microwave and radiofrequency curing of polymers – energy-requirements, cost and market penetration. Energy 1989;14(12):839–51.

[61] Bhattacharya M, Basak T. Detailed material-invariant analysis on spatial resonances of power absorption for microwave-assisted material processing with distributed sources. Industrial and Engineering Chemistry Research 2007;46:750–60.

[62] Bhattacharya M, Basak T. New closed form analysis of resonances in microwave power for material processing. AIChE Journal 2006;52:3707–21.

[63] Basak T, Kumaran SS. A generalized analysis on material invariant characteristics for microwave heating of slabs. Chemical Engineering Science 2005;60(20):5480–98.

[64] Ayappa KG, Davis HT, Crapiste G, Davis EA, Gordon J. Microwave heating: an evaluation of power formulations. Chemical Engineering Science 1991;46(4): 1005–16.

[65] Balanis CA. Advanced engineering electromagnetics. New York: Wiley; 1989.

[66] Stuerga DAC, Gaillard P. Microwave athermal effects in chemistry: a myth's autopsy .2. Orienting effects and thermodynamic consequences of electric field. Journal of Microwave Power and Electromagnetic Energy 1996;31(2): 101–13.

[67] Herrero MA, Kremsner JM, Kappe CO. Nonthermal microwave effects revisited: on the importance of internal temperature monitoring and agitation in microwave chemistry. Journal of Organic Chemistry 2008;73(1):36–47.

[68] Gerasev AP. Simulation of catalytic processes in a fixed bed with the use of microwave radiation for performing an endothermic reaction. Kinetics and Catalysis 2011;52(6):907–13.

[69] Yeo YK, Kim HY, Kim IW, Moon II , Chung Y, Levdansky VV. Analysis of catalytic reaction systems under microwaves to save energy. Korean Journal of Chemical Engineering 2003;20(1):1–7.

[70] Perry WL, Datye AK, Prinja AK, Brown LF. Microwave heating of endothermic catalytic reactions: Reforming of methanol. AIChE Journal 2002;48(4):820–31.

[71] Shin GI, Yeo YK, Jo BY, Kim HY, Levdansky VV. Analysis on effects of microwave heating in porous catalysts. Journal of Chemical Engineering of Japan 2001;34(12):1567–74.

[72] Pipus G, Plazl I, Koloini T. Esterification of benzoic acid in microwave tubular flow reactor. Chemical Engineering Journal 2000;76(3):239–45.

[73] Plazl I, Pipus G, Koloini T. Microwave heating of the continuous flow catalytic reactor in a nonuniform electric field. AIChE Journal 1997;43(3):754–60.

[74] Bhattacharya M, Basak T, Senagala R. A comprehensive theoretical analysis for the effect of microwave heating on the progress of a first order endothermic reaction. Chemical Engineering Science 2011;66:5832–51.

[75] Bhattacharya M, Basak T, Ayappa KG. A fixed grid finite element based enthalpy formulation for generalized phase change problems: role of superficial mushy region. International Journal of Heat and Mass Transfer 2002;45: 4881–98.

[76] Ayappa KG, Davis HT, Davis EA, Gordon J. Analysis of microwave-heating of materials with temperature-dependent properties. AIChE Journal 1991;37(3): 313–22.

[77] Fricke H. The complex conductivity of a suspension of stratified particles of spherical or cylindrical form. Journal of Physical Chemistry 1955;59:168–70.